PILLAR DESIGN AND COAL STRENGTH

By Christopher Mark, Ph.D.,[1] and Timothy M. Barton[1]

ABSTRACT

A comprehensive data base was created that includes more than 4,000 individual uniaxial compressive strength test results from more than 60 coal seams. These data were compared with 100 case studies of in-mine pillar performance from the Analysis of Retreat Mining Pillar Stability (ARMPS) data base.

Statistical analysis found no correlation between the ARMPS stability factor of failed pillars and coal specimen strength. Pillar design was much more reliable when a uniform coal strength of 6.2 MPa (900 psi) was used in all case histories. The conclusion is that laboratory testing should *not* be used to determine coal strength for ARMPS.

Other analyses provided evidence of why laboratory strength does not correlate with pillar strength. The data showed clearly that the "size effect" observed in laboratory testing is related to coal structure. The widely used Gaddy formula, which predicts a significant strength reduction as the specimen size is increased, was found to apply only to "blocky" coals. For friable coals, the size effect was much less pronounced, or even nonexistent. Laboratory tests do not account for large-scale discontinuities, such as roof and floor interfaces, which apparently have more effect on pillar strength than small-scale structure.

[1]Mining engineer, Pittsburgh Research Center, National Institute for Occupational Safety and Health, Pittsburgh, PA.

BACKGROUND

The uniaxial compressive strength of coal was one of the first issues addressed by early rock mechanics researchers. Bunting [1911] observed that "to mine without adequate pillar support will result, sooner or later, in a squeeze; the inherent effects of which are crushing of the pillars, the caving of the roof, and the heaving of the bottom." By testing anthracite specimens of various sizes and shapes in the laboratory, Bunting and his collaborators hoped to aid mine operators in "establishing the width of chambers and pillars." They soon found that "the crushing strength of small cubes is greater than that for large cubes; and, with a constant base area, the crushing strength becomes less as the height increases" [Daniels and Moore 1907]. Bunting apparently concluded that these two issues, the "size effect" and the "shape effect," prevented the direct use of laboratory strength results in design. His design equation was the first U.S. empirical coal pillar strength formula:

$$S_p = S_1 [0.70 + 0.30(w/h)], \quad (1)$$

where S_p = pillar strength,

S_1 = coal strength parameter,

w = pillar width,

and h = pillar height.

Bunting used the laboratory results to determine the *shape* of the formula (figure 1). The coal strength parameter was determined from analysis of in situ pillar failure ("actual squeezes" in figure 1). For anthracite pillars, it was set at 7 MPa (1,000 psi).

The basic approach employed by Bunting and his colleagues remained the state of the art for much of the 20th century. For example, Zern presented the following equation in the 1928 edition of the "Coal Miner's Pocketbook":

$$S_p = S_1 (w/h)^{0.5}. \quad (2)$$

Zern's suggested value of the coal strength parameter is 4.8-7 MPa (700-1,000 psi).

More than 20 years later, Gaddy [1956] attempted to provide the link between laboratory specimens and field strength. He attacked the size effect by testing coal cubes of various sizes from five seams. Gaddy concluded that the strength decrease with increasing specimen size could be expressed as

$$k = S_c (d)^{-0.5}, \quad (3)$$

where k = Gaddy constant
= estimated strength of a 2.5-cm (1-in) cube,

S = coal specimen strength,

and d = specimen dimension (in).

His work led to the widely used Holland-Gaddy pillar strength formula [Holland and Gaddy 1956]:

$$S_p = k (w)^{0.5}/h. \quad (4)$$

The Holland-Gaddy formula appears to have been the first in the United States to employ a seam-specific strength parameter determined from laboratory testing.

In situ testing of full-scale pillars in South Africa during the 1960's resulted in the concept of a "critical" specimen size beyond which the strength is constant [Bieniawski 1968]. The Bieniawski pillar strength formula below employed this concept:

$$S_p = S_1 [0.64 + 0.36(w/h)], \quad (5)$$

where S_1 = in situ coal strength.

Following Hustrulid [1976], Bieniawski recommended that the in situ strength be determined from laboratory tests and that the Gaddy formula be used to reduce the strength to that of a 1-m (36-in) critical-sized specimen [Bieniawski 1984].

Others proposed versions of the Holland-Gaddy and Obert-Duvall (Bauschinger) formulas that employed the in situ strength parameter [Bieniawski 1984]. It may be noted that the in situ coal strength in equation 5 is functionally equivalent to the "coal strength parameter" in equations 1 and 2.

Despite the fact that textbooks have considered laboratory testing an integral part of pillar design for nearly 30 years, it has remained controversial. One reason is that coal remains notoriously difficult to test. Coal contains many types of discontinuities, including microfractures, cleats, bedding planes, partings, shears, and small faults. Three sources of unreliability have been identified:

1. *Material variability within a particular seam:* Unrug et al. [1985] tested multiple layers of the Warfield and the Coalburg Seams and found that the strongest layers were *six times* stronger than the weakest in each seam. Newman and Hoelle [1993] reported similar results from the Harlan Seam.

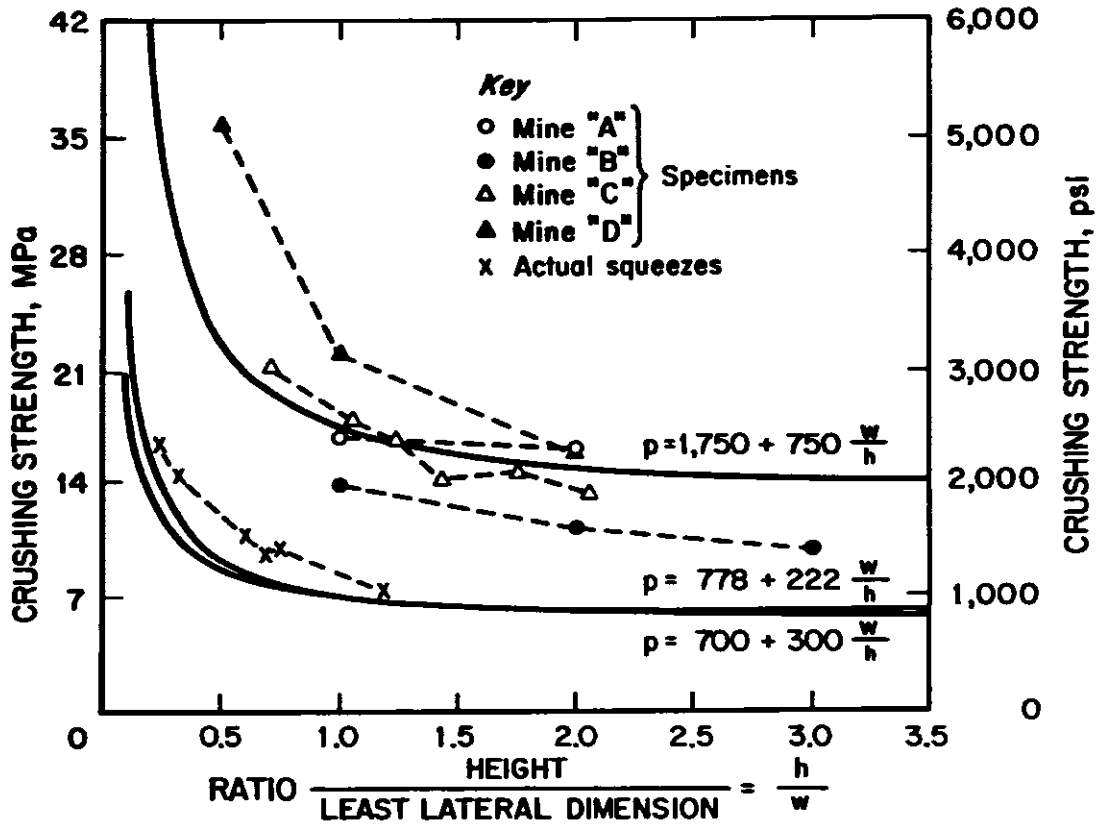

Figure 1.—Data used to develop the first U.S. pillar strength formula (after Bunting, [1911]).

2. *Variation in sampling, specimen preparation, and testing techniques:* Townsend et al. [1977] found that small cylindrical specimens were typically 30% weaker than cubical specimens of the same cross-sectional area. Khair [1968] documented large effects due to platen friction.

3. *Variation in size and shape effects between seams:* Panek [1994] and Mrugala and Belesky [1989], among others, have speculated that Gaddy's size effect exponent of −0.5 may be the *maximum* and not universally applicable. The shape effect has been the subject of numerous studies.

Some have held that these difficulties and the resulting high variability in results are enough to largely invalidate laboratory testing. Another school of researchers in the Republic of South Africa, Australia, and the United States have argued that, although the strength of laboratory-sized specimens varies widely, the in situ coal strength may fall within a narrow range [Salamon 1991; Galvin 1995; Mark 1990]. In each case, their conclusions were based on analysis of in-mine pillar failures. Salamon and Munro [1967] originally analyzed 27 pillar collapses and 92 intact cases. Their formula, perhaps the most widely used in the world, explained the data very well without reference to individual seam strengths. In 1991, Madden reanalyzed an updated version of their data set. Although he found some differences in strength between seams, he concluded again that the average strength could represent all seams. Galvin [1995] conducted a probabilistic analysis of 30 collapsed and stable bord-and-pillar workings from Queensland and New South Wales, Australia. He concluded that "pillar strength in the field is only marginally dependent on the seam strength once the w/h exceeds 2." In the United States, Mark and Chase [1997] presented data from 140 case histories, which were analyzed using the Analysis of Retreat Mining Pillar Stability (ARMPS). ARMPS estimates pillar strength using a slightly modified version of the Bieniawski formula; the analyses assumed a uniform in situ coal strength. Mark and Chase [1997] found that pillar failures occurred in 83% of cases when the ARMPS stability factor (SF) was less than 0.75, but only 8% of cases when it greater than 1.5 (figure 2).

These researchers have all determined that the value of the in situ coal strength falls between 5.4-7.4 MPa (780-1,070 psi). The range is remarkably small, considering that it was determined from three data sets that span the globe. On the other hand, at least one South African seam has been shown by back-calculation to be significantly weaker than the average [Van der Merwe 1993]. In India, researchers concluded from back-analysis of 43 pillar case histories that coal strength should be considered in design [Sheorey et al. 1987].

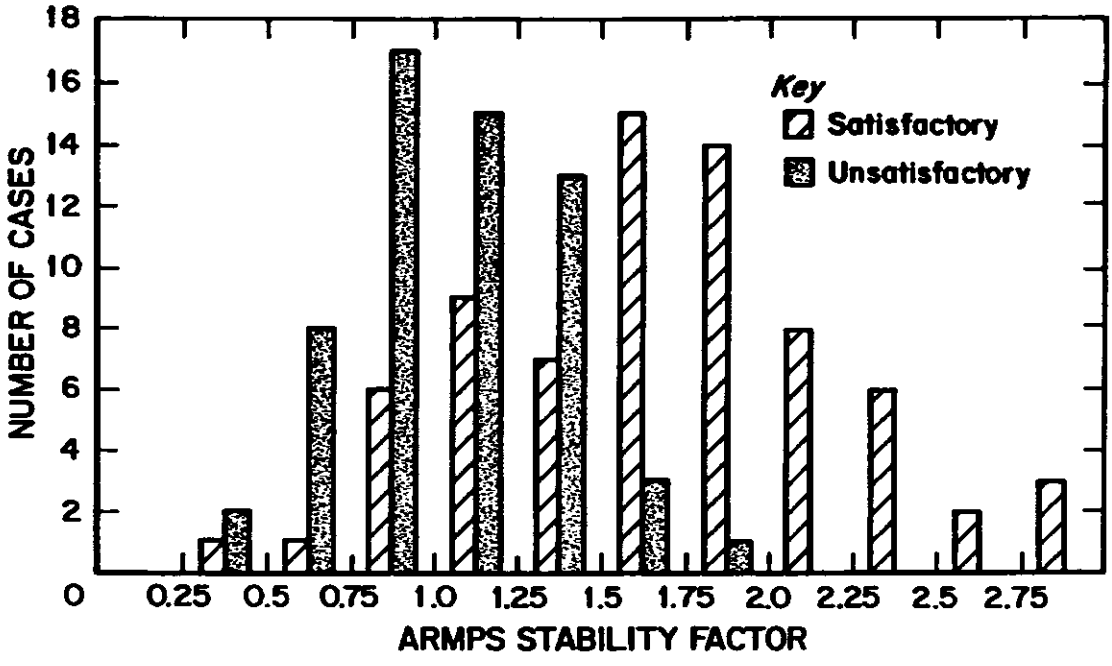

Figure 2.—ARMPS data base.

Interest in the uniaxial compressive strength of coal has also waned over the past 15 years because researchers have devoted their energy to analytic pillar strength formulas and numerical models. These theories are developed from the principles of mechanics rather than curve-fitting to test data. The shift in emphasis has been related to the recent focus on pillar design for longwall mining. Longwalls employ pillars that are much more "squat" than those traditionally used in room-and-pillar operations. Few compressive strength tests have ever been conducted where the specimen width-to-height (w/h) ratio exceeded 4; however, longwall pillars often employ w/h ratios of 10, 20, or greater.

Obviously, the very concept of pillar failure takes on a different meaning for squat pillars. The wide range of conflicting theories about the mechanics of squat pillars and the substantial difficulties with obtaining field data to confirm or disprove any of them have been described elsewhere [Mark and Iannacchione 1992]. On the other hand, Mark et al. [1994] have shown that longwall tailgate performance can be accurately predicted without reference to seam-specific coal strength. There is clearly overwhelming evidence, theoretical and empirical, that the uniaxial compressive strength is irrelevant to the strength of a squat pillar.

Longwall mines, however, account for only 45% of the coal mined underground in the United States. Much of the remainder comes from small room-and-pillar mines usually operating at relatively shallow cover. These mines use many "slender" pillars, and traditional pillar failures still occur. The ARMPS data base contains 60 instances of pillar squeezes, bumps, or collapses that have taken place in recent years. About one-half of these occurred at depths of less than 150 m (500 ft) and involved pillars whose w/h ratio was less than 5. The failures occurred in a variety of seams. Because some seams appear blocky and strong, and others seem weak and extremely friable, it is reasonable to expect that these obvious structural differences might affect pillar strength. As figure 2 shows, successful and unsuccessful designs occur in approximately equal proportions in the ARMPS SF range of 0.75 to 1.5. Might seam-specific laboratory coal strength data explain some of this variability? That was the question this research was initiated to answer.

DISCUSSION OF RESEARCH

Despite the large volume of coal strength testing reported in the literature, it had never been compiled into a single data base. The Pittsburgh Research Center, therefore, undertook the task. The Coal Strength Data Base now contains the results from more than 4,000 individual uniaxial compressive strength tests covering more than 60 seams and obtained from more than 30 references. All of the data have been entered into a spreadsheet and are readily accessible for a wide variety of statistical studies.

Two types of data are included. For about 2,300 tests, information was provided on single specimens. These data were entered individually, then grouped by reference, seam,

specimen geometry, and specimen size. Each group, or suite, of tests was placed on a separate page within the data base. A "summary line" containing the mean compressive strength and standard deviation for the suite was also generated. The summary lines were collected and placed in the summary table. The summary table also includes lines representing about 1,700 tests that were reported in summary form in the original reference. The summary table contains information on about 380 suites of tests. The structure of the Data Base of Uniaxial Coal Strength (DUCS) is illustrated in figure 3.

A single copy of the DUCS may be obtained by sending three formatted, double-sided, high-density diskettes to: Timothy M. Barton, NIOSH, Pittsburgh Research Center, Cochrans Mill Rd., P.O. Box 18070, Pittsburgh, PA 15236-0070. Please specify whether you prefer .xls, .wk3, or comma-separated values format.

A table of average U.S. coalbed strengths was derived from the summary statistics (table 1). To minimize size and shape effects, this table uses only specimens whose w/h ratio is approximately 1.0 and whose smallest dimension is approximately 5-8 cm (2-3 in). The average coalbed strength is calculated as the weighted mean of all of the summary lines for a particular seam that meet these geometric criteria. In addition to strength data, the Coal Strength Data Base also includes a variety of coal quality information for each seam tested. The most relevant is perhaps the Hardgrove Grindability Index (HGI), which is a measure of the relative grindability of coal. Larger HGI values imply easier grindability and greater friability. The HGI is almost universally required by utilities that purchase coal, so the information is readily accessible. Representative values of the rank, carbon content, volatile content, ash content, and heating value are also included. Because the coal quality data were collected independently of the coal strength data and from different sources, they are approximations for comparative purposes only.

During the past 6 years, coal samples measuring about 0.003 m^2 (0.1 ft^3) have also been collected from 45 seams. These were classified using the following simple system:

Composition:

Bright (>90% bright coal)
Semibright (60%-90% bright coal)
Intermediate (40%-60% bright coal)
Semidull (60%-90% dull coal)
Dull (>90% dull coal)

Structure:

Blocky (major cleat spacing > 8 cm (3 in))
Semiblocky (major cleat spacing 3-8 cm (1-3 in))
Friable (cleat spacing < 3 cm (1 in))

Shearing: Yes or no.

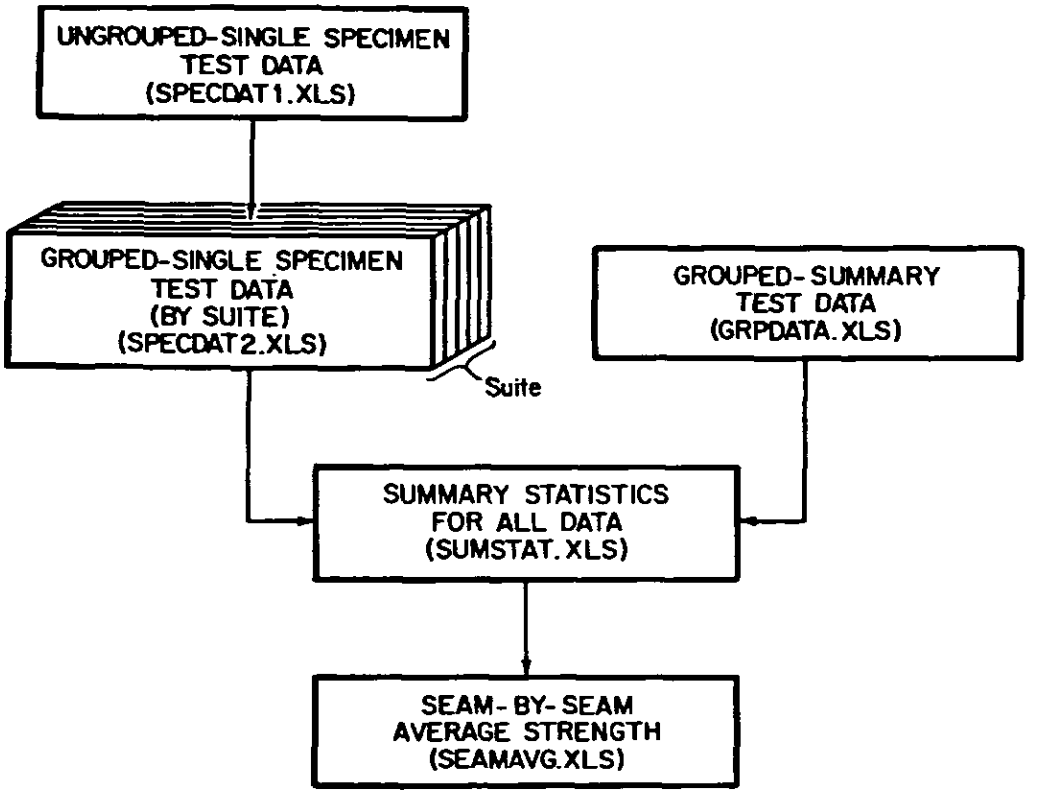

Figure 3.—Structure of the Coal Strength Data Base.

Table 1.—Unconfined compressive strength of U.S. coal seams (5- to 8-cm (2- to 3-in) specimens)

Coalbed	Seam average strength, MPa (psi)	Typical HGI	No. of tests	Coalbed	Seam average strength, MPa (psi)	Typical HGI	No. of tests
Allen	10.8 (1,570)	100	11	Kentucky No. 13	26.8 (3,890)	60	37
Alma	27.7 (4,024)	55	30	Lower Kittanning	14.6 (2,117)	90	96
B	25.1 (3,633)	95	61	Marker	44.9 (6,509)	47	24
Bakerstown	16.7 (2,420)	64	12	Mary Lee	7.8 (1,135)	76	10
Beckley	14.6 (2,121)	101	30	No. 2 Gas	12.4 (1,801)	52	50
Blind Canyon	38.9 (5,646)	46	54	Pittsburgh	160 (4,330)	56	160
Blue Creek	9.1 (1,324)	81	10	Pocahontas No. 3	10.5 (1,528)	110	85
Chilton	27.4 (3,973)	50	6	Pocahontas No. 4	19.9 (2,892)	90	31
Clintwood	19.2 (2,783)	63	40	Pocahontas No. 5	14.7 (2,127)	100	4
Coalburg	24.3 (3,521)	45	124	Pond Creek	32.0 (4,635)	39	13
D	18.2 (2,632)	46	10	Powellton	13.8 (2,008)	58	13
Darby	20.9 (3,907)	49	22	Redstone	20.2 (2,932)	65	10
Douglas	15.9 (2,300)	50	7	Sewell	16.5 (2,386)	65	30
E	24.2 (3,514)	47	4	Sewickley	27.6 (4,000)	60	72
Eagle	10.5 (1,526)	59	10	Stockton	47.2 (6,844)	45	10
Elkhorn No. 4	30.3 (4,393)	42	24	Sunnyside	26.6 (3,856)	50	48
Geneva	36.2 (5,250)	48	3	Tiller	15.3 (2,215)	54	12
Harlan	32.6 (4,728)	44	88	Upper Banner	9.6 (1,391)	84	30
Hazard No. 4	18.2 (2,644)	43	67	Upper D	46.5 (6,746)	50	36
Hernshaw	32.6 (4,727)	47	10	Upper Freeport	10.3 (1,493)	82	17
Herrin No. 6	24.7 (3,576)	57	102	Upper Hiawatha	37.6 (5,446)	46	20
Island Creek	32.6 (4,734)	42	8	Upper Kittanning	10.5 (1,519)	79	60
Jawbone	3.7 (539)	54	3	Warfield	22.7 (3,295)	50	93
Kellioka	21.8 (3,159)	44	49	Waynesburg	30.9 (4,474)	54	15
Kentucky No. 9	28.3 (4,102)	54	46	Welch	13.1 (1,902)	95	6
Kentucky No. 11	25.5 (3,693)	52	52	Winfrede	43.8 (6,345)	45	10
Kentucky No. 12	15.6 (2,268)	58	5	York	18.9 (2,735)	54	60

The ARMPS data base contains the best available information on the in situ strength of U.S. coal pillars. ARMPS SF have been back-calculated for 140 case histories (figure 2), covering an extensive range of geologic conditions, extraction methods, depths of cover, and pillar geometries [Mark and Chase 1997]. Ground conditions in each case history have been categorized as either satisfactory or unsatisfactory. Unsatisfactory conditions included—

- Pillar squeezes, with significant entry closure and loss of reserves.
- Sudden collapses of groups of pillars, usually accompanied by airblasts.
- Coal pillar bumps (violent failures of one or more pillars).

RESULTS

ARMPS CASE HISTORY DATA BASE

Coalbed specimen strength data were available for approximately 100 case histories in the ARMPS data base. The case histories are about evenly split between successes and failures. In figure 4, the ARMPS SF are plotted against coal strength. All ARMPS SF were calculated assuming the in situ strength was 6.2 MPa (900 psi). If pillar strength was related to specimen strength, low-strength seams would be expected to fail at greater SF than high-strength seams. Instead, no meaningful correlation between SF and coal strength is apparent in the data. The best discrimination is achieved at an ARMPS SF of 1.55, with a misclassification rate of 20%. Only one failure is included among the misclassifications, which is highly significant from a practical standpoint.

In a second analysis, the ARMPS SF were recalculated using individual seam strengths instead of the uniform in situ strength. The seam strengths were divided by 4, as suggested by the Gaddy formula for a 6.5-cm (2.5-in) specimen, resulting in a mean SF that is about the same as in the first analysis.

The results are shown in figure 5. Now there is a strong correlation between specimen strength and SF, with "stronger" coals requiring higher SF to avoid failure. The best misclassification rate, at an SF of about 1.7, is 37%. Also, the misclassifications now include 10 failures. In other words, when seam-specific strengths are used, the SF becomes almost meaningless.

A third analysis applied seam-specific size-effect exponents to the coal strength data, as defined later in the "Size Effect" section of this paper. The correlation between seam strength and SF was still apparent, as in figure 5. Although the misclassification rate improved to 33%, it was still 50% greater than in the uniform seam strength analysis.

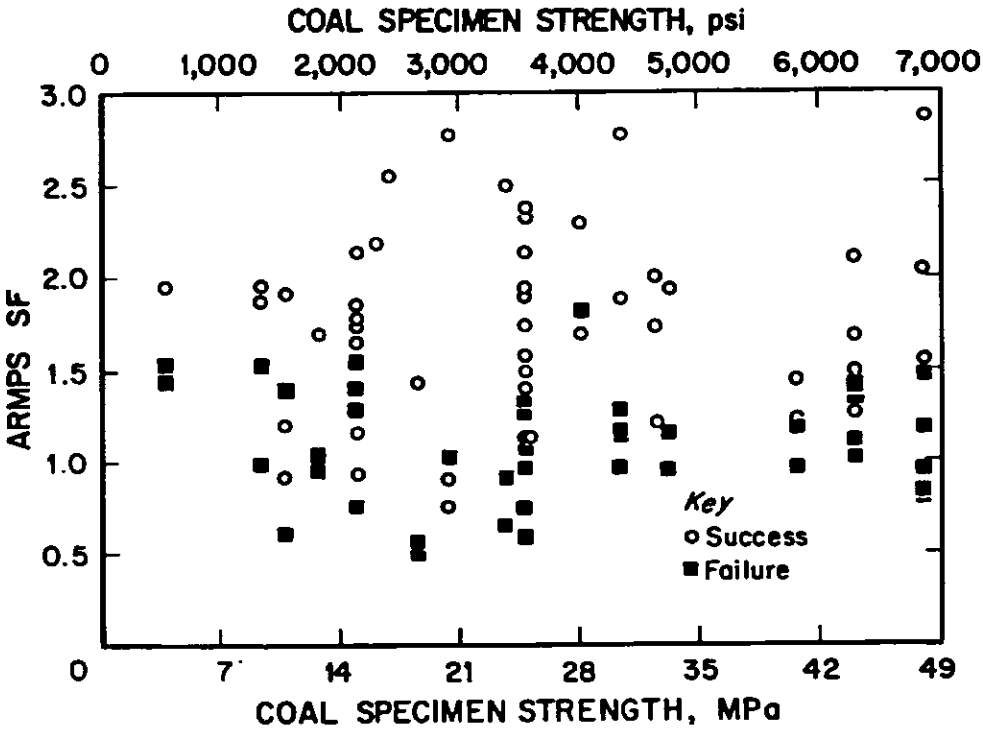

Figure 4.—ARMPS SF compared with specimen strength data.

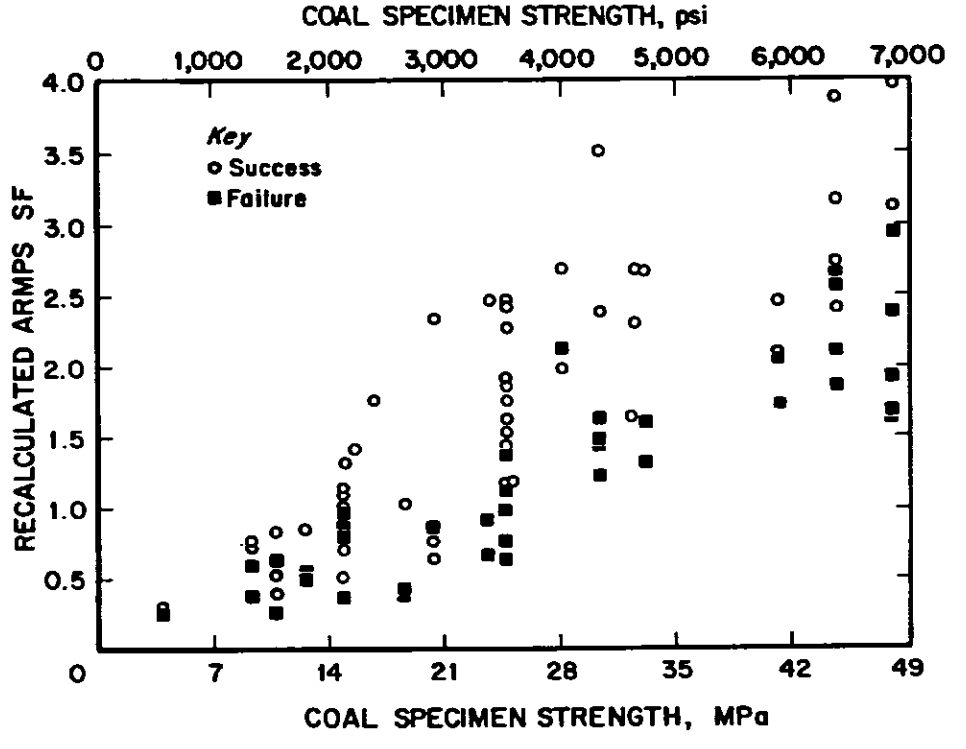

Figure 5.—Recalculated ARMPS SF compared using seam-specific coal strength data.

The data indicate that there is no meaningful correlation between the specimen strength and the in situ strength of U.S. coal seams. Knowledge of the specimen strength does not improve the accuracy of the design formula's prediction; it *reduces* it. A uniform coal strength provides a much more reliable prediction of pillar performance. Based on these results, laboratory test results are explicitly *not* recommended for use in ARMPS.

SIZE EFFECT

The Coal Strength Data Base contains information from 10 seams where a wide range of specimen sizes have been tested. Five of these were the seams originally tested by Gaddy.

To determine the size effect, only specimens with a w/h ratio of approximately 1:1 were used. Figures 6 and 7 show how power curves were fit to the data of the form:

$$S_c = k(d)^{\alpha}, \qquad (6)$$

where α = size effect exponent.

The results are summarized in table 2. Gaddy's α of −0.5 was found to apply to four seams: the Blind Canyon, Elkhorn, Pittsburgh, and Taggart-Marker. At the other extreme, the two Pocahontas Seams displayed negligible size effect. The other four seams had intermediate size effects. The r^2 values indicate that the size effect typically explains about 50% of the variability in the test results, which is higher than expected considering all of the potential sources of variation in these data. The explanation for the substantial range in size effect exponents is the different structure of the coalbeds. In a blocky coalbed, like the Pittsburgh (figure 6), a small sample will be largely free of cleats and fractures. As the specimen size increases, the density of cleating increases until it finally approaches in situ. In contrast, the fracture density of even a small sample of a friable seam like the Pocahontas No. 3 is nearly as great as in situ (figure 7). The following relationship between size effect and HGI was found ($r^2 = 0.75$):

$$\alpha = 0.0063\ \mathrm{HGI} - 0.75. \qquad (7)$$

The implications of seam-specific size effects are quite important. It appears that the Gaddy equation underestimates the in situ strength of most seams, sometimes by a factor of 3 or more. Extremely costly and inefficient mining plans have certainly been the result.

COAL STRUCTURE

Several analyses explored the relationship between coal structure and specimen strength. Figure 8 shows U.S. coalbed strengths plotted against HGI. It shows that specimens from all seams with HGI > 70 have strengths less than 20 MPa (3,000 psi). These seams include all of the medium- and low-volatile seams in the data base. Likewise, 85% of seams with HGI < 50 have a strength exceeding 20 MPa (3,000 psi). For the large number of seams between these extremes, the HGI is a poor predictor of strength. Many of these intermediate HGI seams are high-volatile A in rank. The r^2 for the power curve fit to the entire data set is 0.33.

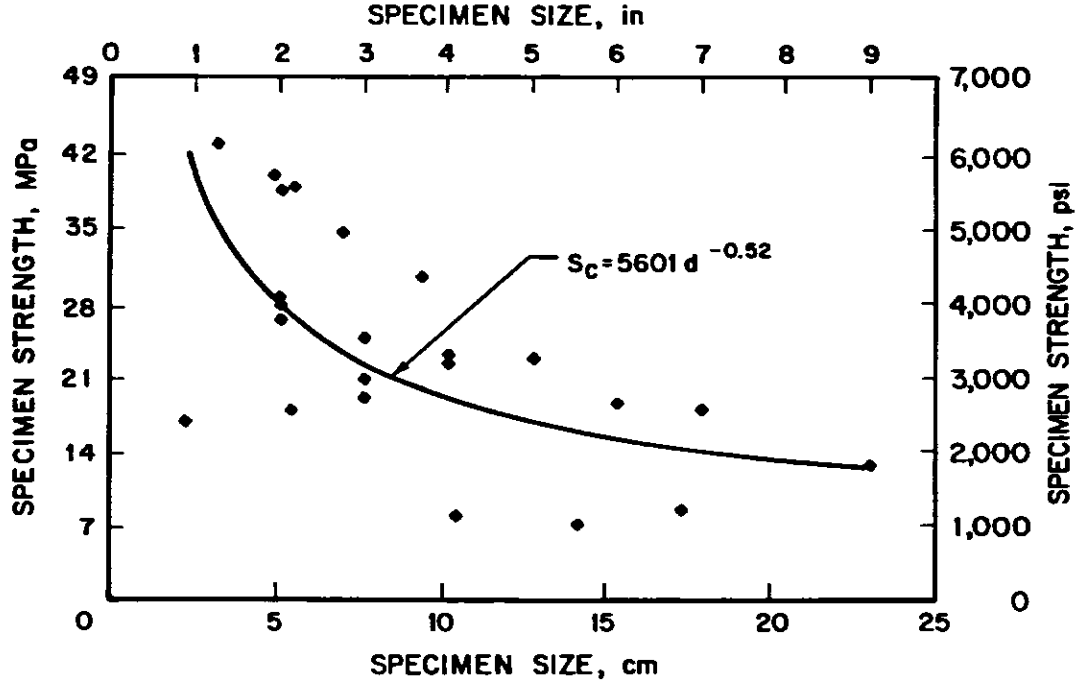

Figure 6.—Size effect in the blocky Pittsburgh Seam.

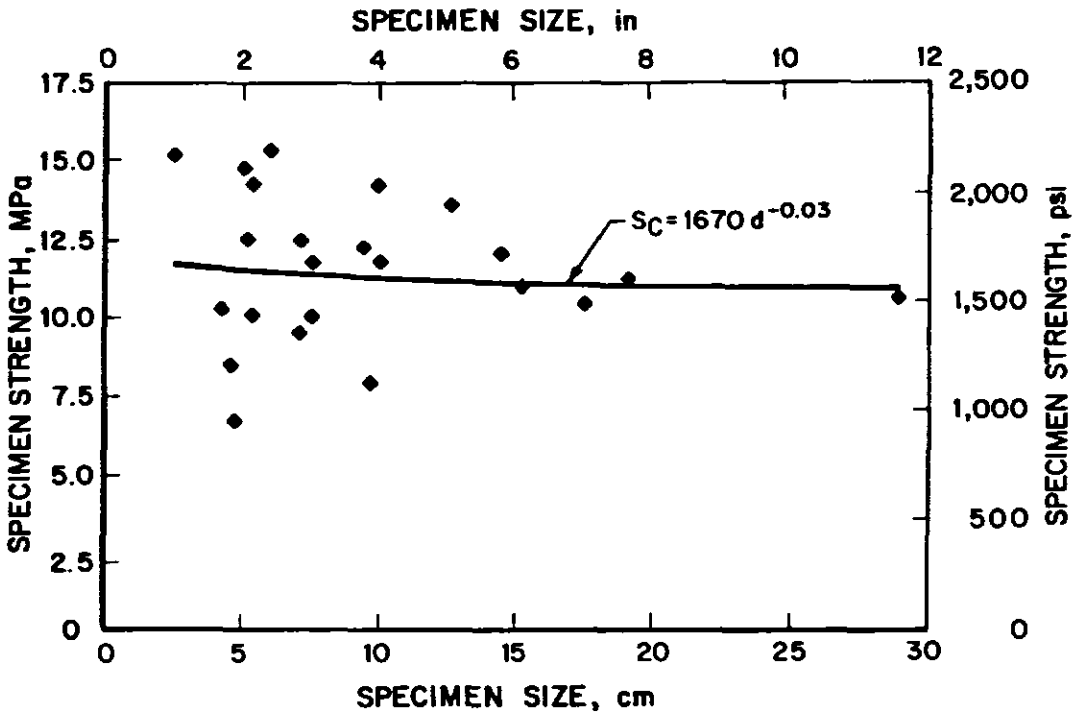

Figure 7.—Size effect in the friable Pocahontas No. 3 Seam.

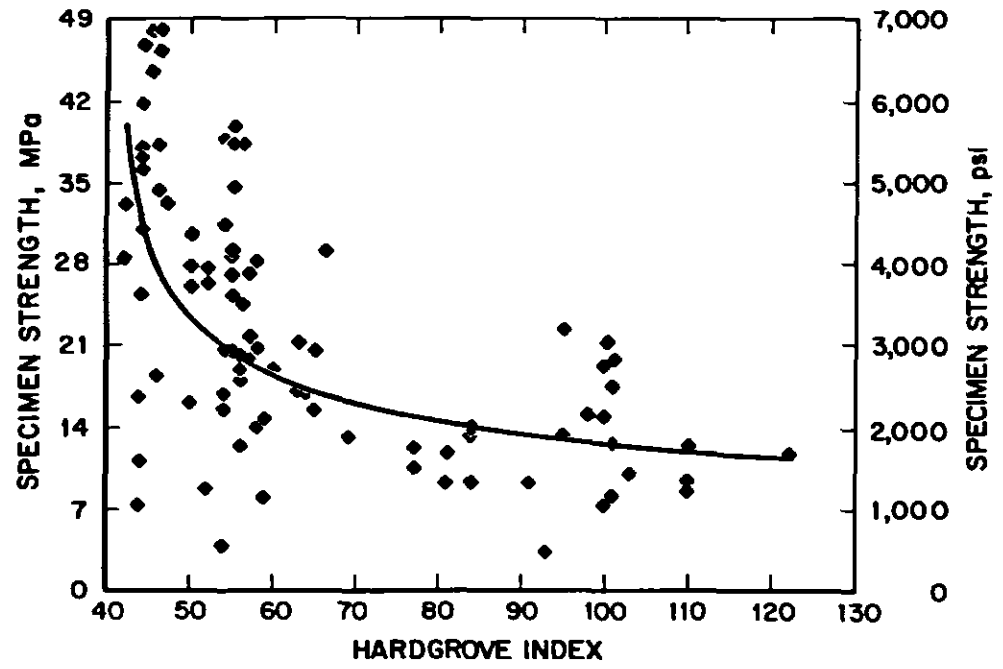

Figure 8.—Specimen strength and HGI of U.S. coalbeds.

Table 2.—Size effect exponents for 10 U.S. coal seams

Coalbed	No. of specimens	No. of references	Maximum specimen size, cm (in)	HGI	Size effect (α)	k	r^2
Blind Canyon	126	2	29.5 (11.6)	46	-0.54	7,045	0.90
Clintwood	88	1	18 (7)	63	-0.31	3,686	0.93
Elkhorn	69	1	16.0 (6.3)	42	-0.55	7,302	0.52
Harlan	129	2	18 (7)	44	-0.29	6,491	0.31
Herrin No. 6	150	5	34.5 (13.6)	56	-0.38	4,293	0.33
Taggart-Marker	60	1	18 (7)	47	-0.45	9,837	0.99
Pittsburgh	272	7	22.9 (9.0)	55	-0.52	5,601	0.48
Pocahontas No. 3	140	5	29.5 (11.6)	110	-0.03	1,670	0.01
Pocahontas No. 4	74	1	18 (7)	100	-0.13	3,238	0.58
Upper Banner	78	1	20.8 (8.2)	84	-0.29	1,730	0.34

The second analysis compared the structure of the hand samples obtained from the mines with the HGI. In this case, every seam rated "blocky" had an HGI less than 60. The HGI of the "semiblocky" seams was less than 80. "Friable" seams were found throughout the range of HGI.

Compressive strength and sample structure data were available for 26 seams. The specimen strength of all eight blocky seams exceeded 23 MPa (3,500 psi), but so did that of four friable and one semiblocky seam. Another 13 friable and semiblocky seams were intermixed below 23 MPa (3,500 psi).

CONCLUSIONS

The results of this study cast doubt on many textbook assumptions about the value of coal strength testing. The data clearly show that specimen strength and the "size effect" are highly seam-specific and related to coal structure. The widely used Gaddy formula, which applies a uniform strength reduction for all seams as specimen size is increased, only applies to "blocky" coals with cleats spaced more than 8 cm (3 in) apart. For friable coals, the size effect was much less pronounced, or even nonexistent.

Case histories of failed pillars are the best available data on in situ coal strength. This study found no correlation between the ARMPS SF of failed pillars and coal specimen strength in the ARMPS data base. In current ARMPS practice, pillars are designed assuming an in situ strength of 6.2 MPa (900 psi) for all seams. When the specimen strength was used instead, the reliability of the ARMPS design method decreased substantially. Australian and South African studies have also found that pillar strength in the field is largely independent of specimen strength.

It should be noted that the coal strength tests were only matched with the seams in the case histories, not with the individual mines. It is also possible that some of the case histories involved roof or floor failure rather than pillar failures. Using a different pillar strength formula might also have changed the results somewhat. However, the data base is so large and the trends so strong that it is highly unlikely that the study is unrepresentative.

The most likely explanation for the results of the study is that specimen and in situ strengths are determined by different parameters. Laboratory tests, particularly those of blocky coals, require a significant amount of fracturing of intact coal. Pillars contain so many cleats and other discontinuities that their failure can occur almost entirely along preexisting fractures. The laboratory tests measure a parameter—the intact coal strength—that is apparently irrelevant to the in situ strength.

The study did not prove that the in situ strength of all U.S. coals is uniform. It only showed that a uniform strength is a better approximation than one based on laboratory testing. There is still significant variability in the ARMPS SF range of 0.75 to 1.5. Recent model studies have indicated that features such as roof and floor interfaces, bedding planes, partings, or weak coal layers have the greatest effects on in situ strength [Iannacchione 1990; Su and Hasenfus 1996]. A rock mass classification, such as the one proposed by Kalamaras and Bieniawski [1993], may prove to be an effective way of evaluating these effects in the field. In the meantime, laboratory uniaxial coal strength test results should not be used for pillar design with ARMPS.

REFERENCES

Bieniawski ZT [1968]. The effects of specimen size on the compressive strength of coal. Intl J Rock Mech Min Sci *5*:325-335.

Bieniawski ZT [1984]. Rock mechanics design in mining and tunneling. Balkema, Rotterdam, pp. 55-92.

Bunting D [1911]. Chamber pillars in deep anthracite mines. Trans AIME *42*:236-245.

Daniels J, Moore LD [1907]. The ultimate crushing strength of coal. Eng Min J, *Aug 10*:263-268.

Gaddy FL [1956]. A study of the ultimate strength of coal as related to the absolute size of cubical specimens tested. VA Polytechnic Bull 112, *Aug*:1-27.

Galvin JM [1995]. Roadway and pillar mechanics workshop: stage 2 - design principles and practice (Course notes). Sydney, New South Wales, Australia: University of New South Wales.

Holland CT, Gaddy FL [1956]. Some aspects of permanent support of overburden on coal beds. In: Proceedings of the West Virginia Coal Mining Institute, pp. 43-65.

Hustrulid WA [1976]. A review of coal pillar strength formulas. Rock Mechanics *8*:115-145.

Iannacchione AT [1990]. The effects of roof and floor interface slip on coal pillar behavior. In: Hustrulid WA, Johnson GA, eds. Proceedings of the 31st U.S. Symposium on Rock Mechanics. Golden, CO: Colorado School of Mines, pp. 153-160.

Kalamaras GS, Bieniawski ZT [1993]. A rock mass strength concept for coal seams. In: Proceedings of the 12th Conference on Ground Control in Mining. Morgantown, WV: West Virginia University, pp. 274-283.

Khair AW [1968]. The effects of coefficient of friction on strength of model coal pillar [Thesis]. Morgantown, WV: West Virginia University, Department of Mining Engineering.

Madden BJ [1991]. A re-assessment of coal-pillar design. J South Afr Inst Min Metall *91*:27-37.

Mark C [1990]. Pillar design methods for longwall mining. Pittsburgh, PA: U.S. Department of the Interior, Bureau of Mines, IC 9247.

Mark C, Iannacchione AT [1992]. Coal pillar mechanics: theoretical models and field measurements compared. In: Iannacchione AT, Mark C, Repsher RC, Tuchman RJ, Jones CC, comp. Proceedings of the Workshop on Coal Pillar Mechanics and Design. Pittsburgh, PA: U.S. Department of the Interior, Bureau of Mines, IC 9315, pp. 78-93.

Mark C, Chase FE, Molinda GM [1994]. Design of longwall gate entry systems using roof classification. In: Mark C, Tuchman RJ, Repsher RC, Simon CL, comp. New Technology for Longwall Ground Control; Proceedings: U.S. Bureau of Mines Technology Transfer Seminar. Pittsburgh, PA: U.S. Department of the Interior, Bureau of Mines, SP 01-94, pp. 5-18.

Mark C, Chase FE [1997]. Analysis of retreat mining pillar stability (ARMPS). In: Mark C, Tuchman RJ, comp. Proceedings: New Technology for Ground Control in Retreat Mining. Pittsburgh, PA: U.S. Department of Health and Human Services, Public Health Service, Centers for Disease Control, National Institute for Occupational Safety and Health, IC 9446.

Mrugala MJ, Belesky RM [1989]. Pillar sizing. In: Proceedings of the 30th U.S. Symposium on Rock Mechanics. Morgantown, WV: West Virginia University, pp. 395-402.

Newman DA, Hoelle JL [1993]. The impact of variability in coal strength on mine planing and design - a case history. In: 12th Conference on Ground Control in Mining. Morgantown, WV: West Virginia University, pp. 237-243.

Panek LA [1994]. Scaling mine pillars' size and shape with the psi function. Soc Min Eng AIME preprint 94-52, pp. 1277-1280.

Salamon MDG [1991]. Behavior and design of coal pillars. Australian Coal J *32*:11-22.

Salamon MDG, Munro AH [1967]. A study of the strength of coal pillars. J South Afr Inst Min Metall, *Sept*:55-67.

Sheorey PR, Das MN, Barat D, Prasad RK, Singh B [1987]. Coal pillar strength estimation from failed and stable cases. Intl J Rock Mech Min Sci Geomech Abstr *24*(6):347-355.

Su DWH, Hasenfus GJ [1996]. Practical coal pillar design considerations based on numerical modeling. In: 15th Conference on Ground Control in Mining. Golden, CO: Colorado School of Mines.

Townsend JM, Jennings WC, Haycocks C, Neall GM, Johnson, LP [1977]. A relationship between the ultimate compressive strength of cubes and cylinders for coal specimens. In: Symposium for Rock Mechanics, Keystone, CO, pp. 4A6-1 to 4A6-6.

Unrug KF, Nandy S, Thompson E [1985]. Evaluation of the coal strength for pillar calculations. SME AIME preprint 85-314.

Van der Merwe JN [1993]. Revised strength factor for coal in the Vaal basin. J South Afr Inst Min Metall *93*(3), pp. 71-77.

Zern EN [1928]. Coal miner's pocketbook. McGraw-Hill, NY, 12th ed., pp. 641-645.

A NEW LAMINATED OVERBURDEN MODEL FOR COAL MINE DESIGN

By Keith A. Heasley[1]

ABSTRACT

In the past, numerous boundary-element models of stratified rock masses have been proposed using a homogeneous isotropic elastic overburden. In this paper, it is postulated that a laminated overburden model might be more accurate for describing the displacements and stresses in these stratified deposits. In order to investigate the utility of using a laminated overburden in a boundary-element model, the fundamental mathematical basis of the laminated model is presented and graphically compared with the fundamental behavior of homogeneous isotropic elastic overburden and with field data. Specifically, the stresses and displacements surrounding an idealized longwall panel as determined from the laminated overburden model are presented and compared with results from the homogeneous isotropic overburden and with measured abutment stress data. Additionally, the remote displacements and surface subsidence as calculated by the laminated overburden model are compared with homogeneous isotropic calculations and with measured subsidence data. Finally, the new laminated boundary-element program, LAMODEL, is used to model the underground stresses and displacements, the topographic stresses, and the interseam interactions at a field site. The results of this investigation show that the laminated overburden is more supple, apt to propagate displacements and stress further, and better able to fit observed data than the classic homogeneous isotropic overburden. Ultimately, it is suggested that the laminated model has the potential to increase the accuracy of displacement and stress calculations for a variety of mining situations.

[1]Mining engineer, Pittsburgh Research Center, National Institute for Occupational Safety and Health, Pittsburgh, PA.

INTRODUCTION

If one wishes to perform a mechanical analysis of the geologic structure of a mining operation, there are several broad mathematical techniques available. For instance, one may choose finite-element, boundary-element, discrete-element, finite-difference techniques, and/or hybrid combinations of these techniques. In general, these mathematical techniques have strengths and weaknesses when applied to a specific geologic environment, mining geometry, and material behavior. Naturally, in each practical application the mathematical technique best suited to the prevailing conditions should be applied.

To analyze the displacements and stresses associated with the extraction of tabular deposits, such as coal, potash, and other thin vein-type deposits, the displacement-discontinuity version of the boundary-element technique is frequently the method of choice. In the displacement-discontinuity approach, the mining horizon is treated mathematically as a discontinuity in the displacement of the surrounding media. Thus, only the planar area of the seam is discretized in order to obtain the solution. Often this limited analysis is sufficient, because in many applications only the distributions of stress and convergence on the seam horizon are of interest. In addition, by limiting the detailed analysis to only the seam, the displacement-discontinuity method provides considerable computational savings compared with other techniques that discretize the entire body (such as finite-element, discrete-element, or finite-difference). It is a direct result of this computational efficiency that the displacement-discontinuity method is able to handle problems involving large areas of tabular excavations.

In the original mathematical formulations [Berry 1960; Salamon 1962] and computer implementations [Plewman et al. 1969; Crouch and Fairhurst 1973; Sinha 1979] of the displacement-discontinuity variation of the boundary-element method, the media surrounding the seam were assumed to be homogeneous, isotropic, or transversely isotropic elastic. This basic behavior of the surrounding media provided fairly good seam-level displacement and stress results for South African gold mines [Salamon 1964; Cook et al. 1966] and for U.S. coal mines [Kripakov et al. 1988; Zipf and Heasley 1990; Heasley and Zelanko 1992]. However, it was noted early in the application of the displacement-discontinuity method that the homogeneous isotropic overburden model does not fit measured subsidence data [Berry and Sales 1961]. As an alternative, it was proposed that a laminated model might be more suitable for describing the behavior of stratified coal-measure rocks [Salamon 1961, 1963]. Recently, a laminated overburden model was found to give good results for predicting surface subsidence [Salamon 1989a; Yang 1992]. Because the source of surface subsidence is convergence in the seam, it seems reasonable that a laminated overburden model might also be able to provide more accurate predictions of in-seam displacements and stresses.

If the utility of using a laminated overburden in a displacement-discontinuity model is to be determined, the fundamental mechanical behavior of the laminated model needs to be investigated and compared with both the classic homogeneous isotropic model and field data. In this paper, the stresses and displacements surrounding an idealized longwall panel as determined from the laminated overburden model, the homogeneous isotropic overburden model, and field data are presented and compared. In addition, the remote displacements and surface subsidence as calculated by the two overburden models are compared with measured subsidence data. Lastly, the laminated overburden model is applied to a site study.

FUNDAMENTAL BEHAVIOR

MATHEMATICAL FOUNDATION

The mathematical basis for the laminated model was originally proposed by Salamon in 1961-62 and more recently updated in 1991. Conceptually, the media in the laminated model consist of a horizontal stack of homogeneous isotropic layers where the interfaces between the layers are parallel and free of shear and cohesive stresses, and the vertical stresses and displacements are continuous across the layers. In the "homogeneous stratification" version of the model, all layers have the same elastic modulus (E), Poisson's ratio (v), and thickness (t). Thus, the homogeneous stratification formulation does not allow (or need) the specification of the properties for each individual layer, yet it provides the desired suppleness of the basic laminated model (compared with a homogeneous isotropic elastic model). In addition, the behavior of the rock mass in the laminated model is effectively characterized by two parameters, the elastic modulus and the lamination thickness, whereas the homogeneous isotropic model only has a single effective parameter, the rock mass modulus (the Poisson's ratio has a minor effect in both models).

The mathematical foundation of the laminated model is the theory of thin plates [Salamon 1991]. From this theory, the relationship between the vertical deflection (w) of the middle plane of a horizontal plate and the resultant transverse pressure (p) acting on the plate is defined by

$$D \nabla^4 w(x,y) = p(x,y), \quad (1)$$

where D is the flexural rigidity of a plate:

$$D = \frac{E t^3}{12 (1 - \nu^2)}, \quad (2)$$

and ∇^4 denotes the biharmonic operator in the xy plane, specifically:

$$\nabla^4 = \left(\frac{\partial^4}{\partial x^4} + 2\frac{\partial^4}{\partial x^2 \partial y^2} + \frac{\partial^4}{\partial y^4} \right). \quad (3)$$

From equation 1, the convergence in the seam (S) can be related to the induced stress (σ_i) in the overburden laminae by the following second-order, partial differential equation [Salamon 1991]:

$$\frac{\partial^2 S}{\partial x^2} + \frac{\partial^2 S}{\partial y^2} = \frac{2}{E \lambda} \sigma_i, \quad (4)$$

where the laminae-related value, λ, is defined as

$$\lambda = \sqrt{\frac{t^2}{12 (1 - \nu^2)}}, \quad (5)$$

and σ_i is the vertical, or transverse, stress on the laminae at seam level induced by mining.

PANEL CONVERGENCE

The first step in investigating the fundamental behavior of the laminated model was to analyze the convergence across a two-dimensional slot. This slot can be viewed as an idealized longwall panel with no gob support and rigid ribs. From equation 4, the seam convergence across a two-dimensional slot for the laminated model (S_l) as a function of the distance from the panel centerline (X) can be determined as

$$S_l(X) = \frac{\sqrt{12 (1 - \nu^2)}}{t} \frac{q}{E} (L^2 - X^2). \quad (6)$$

Here, L is the half-width of the slot; q is the primitive vertical stress at the mining horizon, which for an open panel is equal to the induced stress (σ_i). In solving equation 4, it was assumed that the convergence value at the rib side is zero and that the convergence distribution is symmetric about the panel centerline. Also, in this result and the result in equation 7, the stress-free ground surface was ignored.

Jaeger and Cook [1979] provide a comparable equation for the roof-to-floor convergence across a two-dimensional slot with homogeneous isotropic elastic overburden (S_h):

$$S_h(X) = 4 (1 - \nu^2) \frac{q}{E} (L^2 - X^2)^{1/2}. \quad (7)$$

The fundamental difference between these two equations is that the convergence in the laminated model is proportional to the square of the panel span, while the convergence in the homogeneous model is linearly proportional to the span.

In order to plot and compare the convergence computed from equations 6 and 7, some "typical" values were assumed for the geometric and rock mass parameters: a panel width of 200 m (656 ft)(L = 100), an overburden depth (H) of 160 m (525 ft)(q = 4 MPa (580 psi)), a seam height (M) of 2 m (6.6 ft), an elastic modulus of the rock mass (E) of 20 GPa (2.9 million psi), a Poisson's ratio (ν) of the rock mass of 0.25, and a lamination thickness (t) of 15 m (49 ft). Using these values for the parameters, the convergence across the slot for both the laminated and the homogeneous overburden is plotted in figure 1. As expected from the nature of the equations, the laminated overburden is considerably more flexible. In fact, with the given parameters, the laminated overburden exhibits six times the convergence of the homogeneous isotropic overburden.

ABUTMENT STRESS

The next step in investigating the fundamental behavior of the laminated model was to analyze the abutment stress at the edge of a two-dimensional slot. If the seam is assumed to be linear elastic with a modulus of E_s and Poisson's effect is ignored, then the induced stress in the seam for the laminated model is

$$\sigma_i = E_s \frac{S_l}{M}. \quad (8)$$

Then, from equation 4, the in-seam convergence in the laminated model is defined by

$$\frac{d^2 S_l}{dx^2} - \frac{2 E_s}{E \lambda M} S_l = 0, \quad (9)$$

which has a solution (for positive X values):

$$S_l(X) = qL \sqrt{\frac{2M}{E \lambda E_s}} e^{\sqrt{\frac{2E_s}{E \lambda M}}(X-L)}. \quad (10)$$

The associated induced vertical abutment stress (σ_l) in the unmined seam bounding the panel is

$$\sigma_l(X) = qL \sqrt{\frac{2E_s}{E \lambda M}} e^{\sqrt{\frac{2E_s}{E \lambda M}}(X-L)}. \quad (11)$$

The total abutment stress at the edge of a two-dimensional slot in a homogeneous isotropic elastic model (σ_h) is given by [Salamon 1974]:

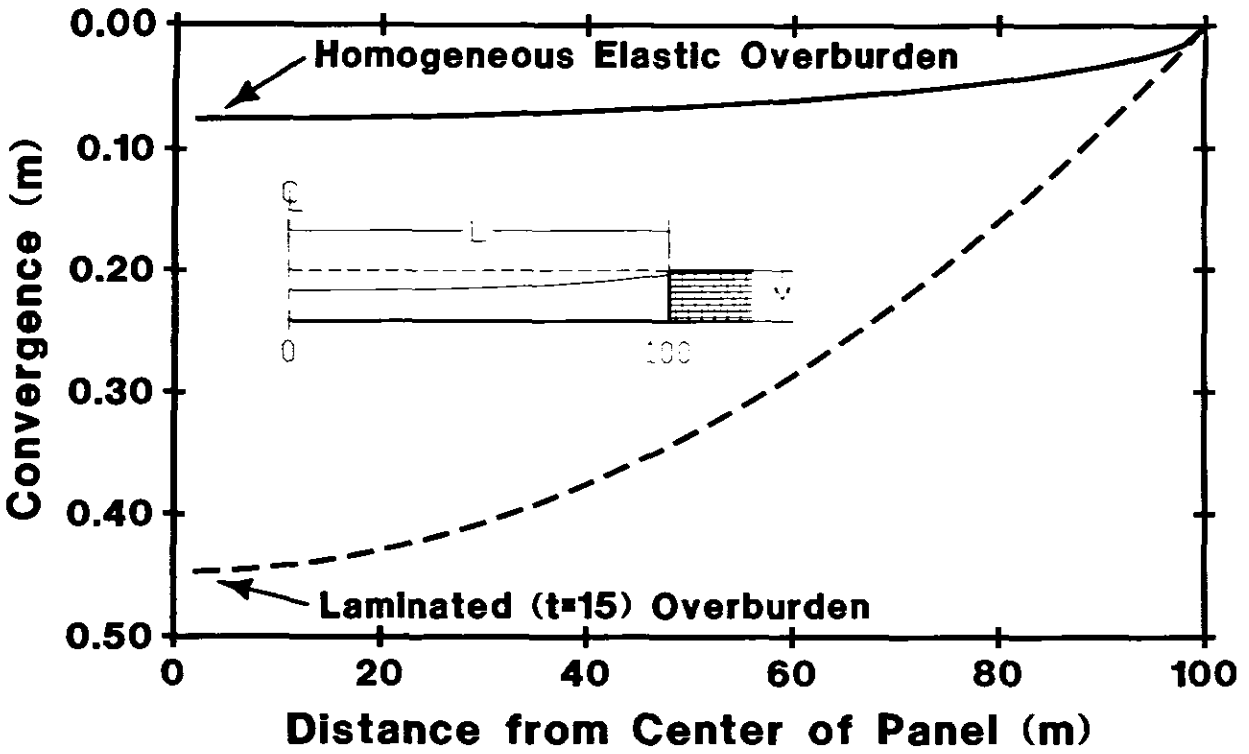

Figure 1.—Comparison of longwall convergence computed from the laminated and homogeneous isotropic models.

$$\sigma_h(X) = \frac{Xq}{\sqrt{X^2 - L^2}}. \qquad (12)$$

It is noteworthy that this equation is independent of material properties. During its derivation, it was assumed that the seam material was identical to the surrounding media. Thus, to be consistent, the elastic modulus of the seam (E_s) in equation 11 is assumed to be equal to the modulus of the overburden (E), 20 GPa (2.9 million psi).

In addition, numerous field measurements of abutment load have been tabulated by Mark [1990], where he found that the measured distribution of induced abutment stress (σ_f) follows the equation:

$$\sigma_f(X) = \frac{3L_s}{(D - L)^3}(D - X)^2, \qquad (13)$$

where L_s is the total side abutment load (which in our case without any gob load is equal to qL), and D is the maximum horizontal extent of the abutment stress from the panel edge, which was determined from field measurements [Mark 1990]:

$$D = L + \sqrt{0.3048}\,(9.3\sqrt{H}). \qquad (14)$$

The total abutment stress curves, as calculated from the laminated and homogeneous isotropic models and from the empirical formula (equations 11, 12, and 13), are plotted in figure 2. (It should be noted that equations 11 and 13 calculate induced stresses and equation 12 calculates the total stress. Therefore, in the following plots, the virgin overburden stress (q) has been added to the results from equations 11 and 13 to provide a valid comparison with the total abutment stress values from equation 12.) In figure 2, it can be seen that the homogeneous isotropic abutment stress has a relatively sharp, infinite peak at the edge and approaches zero asymptotically with increasing distance from the panel. In contrast, the abutment stress in the laminated overburden is finite at the panel edge and approaches virgin overburden stress (q) rapidly. Neither of these mathematical models (using the assumed parameters) comes very close to matching the empirical abutment stress.

However, if the abutment stress level in the laminated model and that obtained from the empirical formula are equated at the edge of the seam (X = L), then the lamination thickness (t) that ensures this equality can be determined:

$$t = 20.29\sqrt{1 - \nu^2}\,\frac{E_s H}{ME}. \qquad (15)$$

For a typical seam modulus (E_s) of 2 GPa (290,000 psi) in the laminated model, equation 15 provides a fitted lamination thickness of 157 m (515 ft). The plot of the abutment stress curve for the laminated overburden model with a fitted lamination thickness of 157 m (515 ft) is shown together with the empirically determined abutment stress in figure 3. The degree of agreement between the two curves is very good and serves to

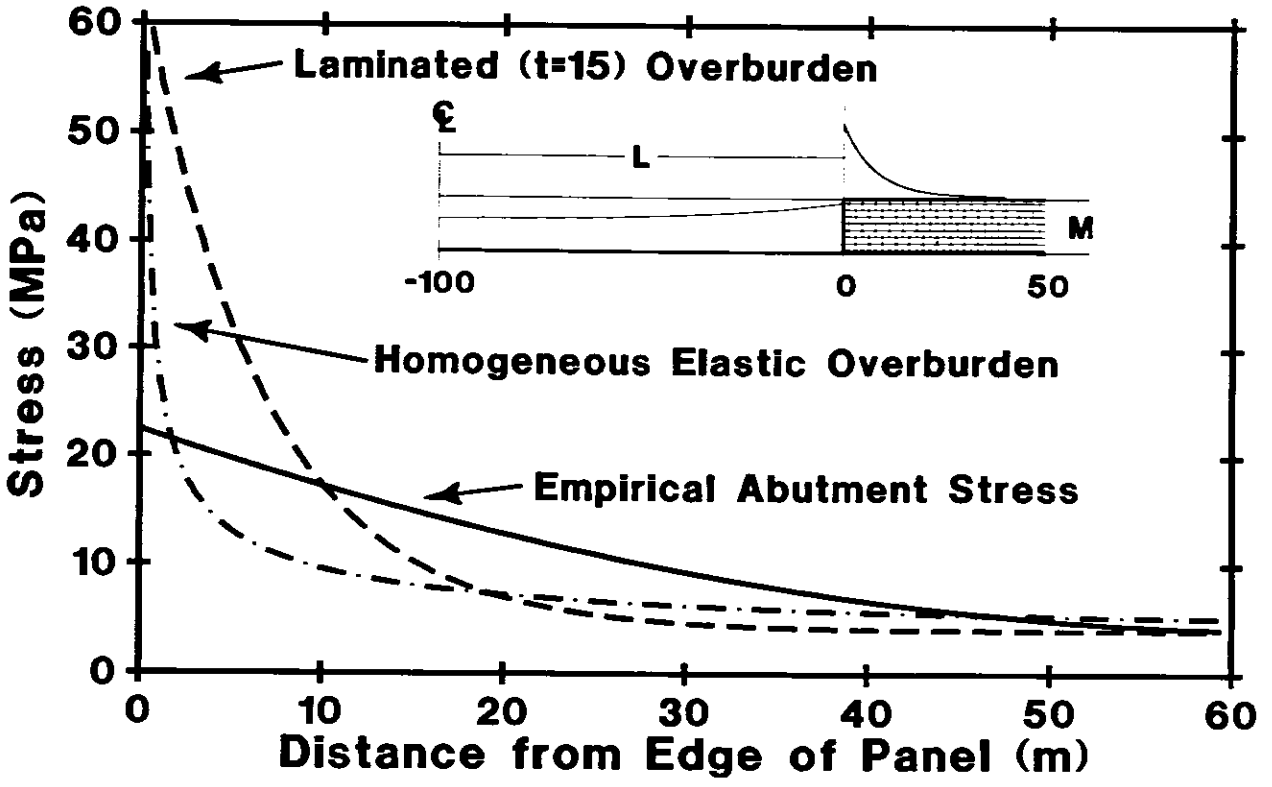

Figure 2.—Comparison of longwall abutment stress computed from the laminated and homogeneous isotropic models and from the empirical formula.

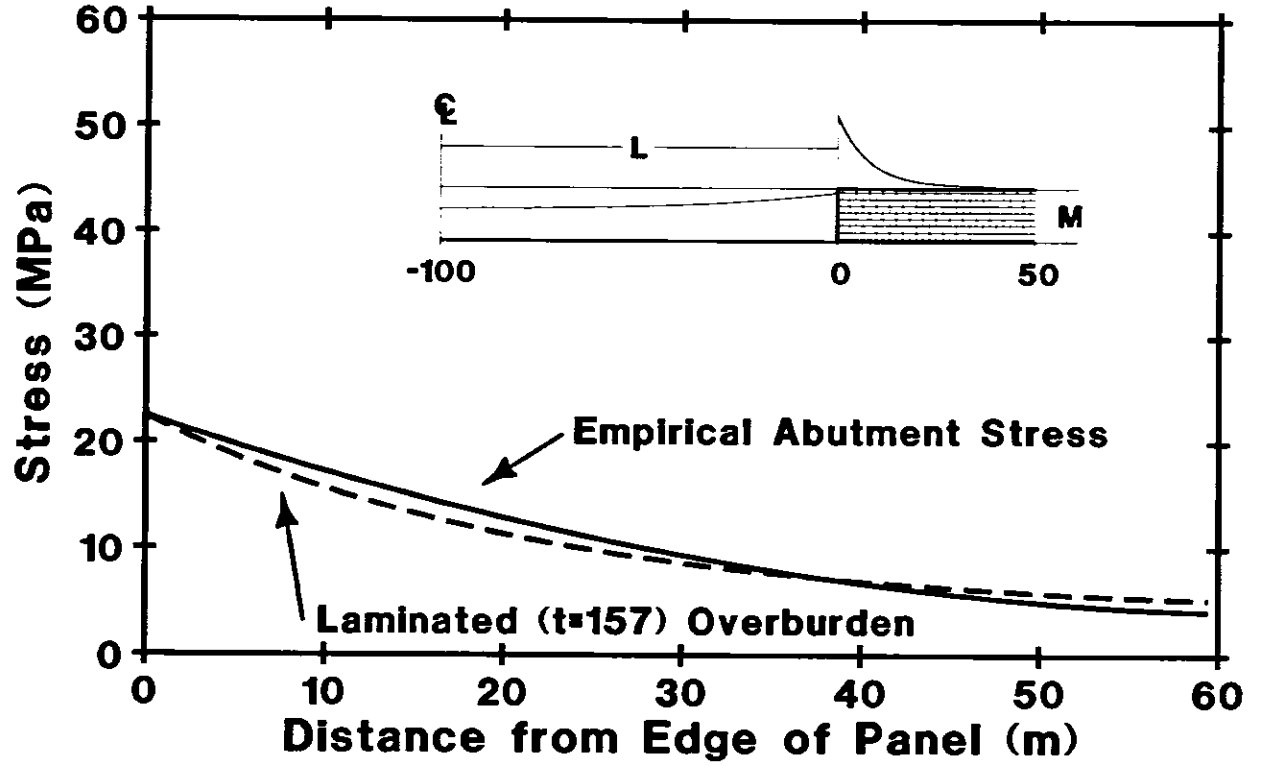

Figure 3.—Plot of the laminated abutment stress fitted to the empirical formula.

highlight the numerical flexibility provided by a variable lamination thickness parameter in the laminated model. (If a compressible seam is used, it may be possible to fit the abutment stress distribution in the homogeneous isotropic overburden to the empirical curve by varying the seam and overburden moduli. However, that calculation is beyond the scope of this paper.)

REMOTE DISPLACEMENTS

The next step was to analyze the remote displacements in the overburden generated by seam convergence. For the laminated overburden model, the kernel, or influence function, which relates the seam convergence (S_f) to the vertical displacement (W_f) of the overburden, was derived by Salamon [1962, 1989b] and Yang [1992]:

$$W_f(X,Y) = \frac{S_f}{4\sqrt{\pi \lambda Y}} e^{\frac{X^2}{4\lambda |Y|}}. \qquad (16)$$

Here, the magnitude of the convergence, S_f, is assumed to occur over a unit element of the seam; the values of X and Y are the horizontal and vertical distances between the centroid of the converged seam element and the point in the overburden at which the displacement is desired.

Similarly, the kernel for the homogeneous isotropic overburden, which relates the seam convergence (S_h) to the vertical displacement (W_h) of the overburden, was derived by Crouch [1976] (see equation 17). Again, the magnitude of the convergence, S_h, is assumed to occur over a unit element of the seam, and the coordinates X and Y were defined previously in conjunction with equation 16. Note that the expression in equation 17 is again independent of elastic moduli.

Plots of the overburden displacements generated by these models are depicted in figure 4 for Y = 20 m (66 ft) and Y = 50 m (164 ft). In computing this illustration, a unit convergence spread over a seam element of unit length was assumed. Thus, the volume of convergence is identical in the two models. However, consistent with the greater suppleness of the laminated model, the stratified overburden (with a 15-m (49-ft) lamination thickness) appears to concentrate the displacement more tightly over the panel. This feature is particularly noticeable as the distance from the seam is increased.

This difference in remote displacement behavior is even more obvious in figure 5, which shows the 1-cm (0.39-in) displacement contours for both models generated above a unit volume convergence in a seam element. In this figure, the 1-cm (0.39-in) contour, or displacement "bulb," for the laminated model (with a 15-m (49-ft) lamination thickness) is broader and extends almost twice the distance into the overburden as the contour from the homogeneous elastic model. However, if the lamination thickness in the laminated model is increased to 28 m (92 ft)(as shown in figure 5), then the vertical extent of the 1-cm (0.39-in) displacement contour is equal between the two models, although the laminated displacement bulb is still broader. For most practical purposes (lower lamination thicknesses), both figures 4 and 5 indicate that seam displacements and stresses for a laminated overburden would propagate further and in a tighter pattern than the displacements and stresses from the homogeneous overburden. This greater remote response, coupled with the tendency for the laminated model to produce greater seam convergence, should greatly increase the remote displacements and stresses associated with a laminated displacement-discontinuity model.

SURFACE SUBSIDENCE

The final step in investigating the fundamental behavior of the laminated model was to analyze the surface subsidence over a longwall panel. In this analysis, the surface subsidence curves for the laminated and homogeneous isotropic models were calculated by taking the panel convergence from equations 6 and 7 and numerically integrating the surface subsidence using equations 16 and 17. These calculated subsidence curves are then compared in figure 6 with the results of the U.S. Bureau of Mines subsidence model [Jeran et al. 1986], which essentially represents an empirically derived "average" of 11 different subsidence curves from the Northern Appalachian Coal Basin.

For the subsidence curve of the laminated model in figure 6, the lamination thickness was optimized to provide the best fit with the empirical curve. This resulted in a lamination thickness of 5.3 m (17 ft), and from the figure, it can be seen that the laminated model provides a good fit to the empirical

$$W_h(X,Y) = \frac{S_h}{2\pi}\left(\arctan\left(\frac{Y}{X-0.5}\right) - \arctan\left(\frac{Y}{X+0.5}\right)\right) + \frac{S_h}{2\pi}\left(\frac{Y}{2(1-\nu)}\left(\frac{X+0.5}{(X+0.5)^2+Y^2} - \frac{X-0.5}{(X-0.5)^2+Y^2}\right)\right), \qquad (17)$$

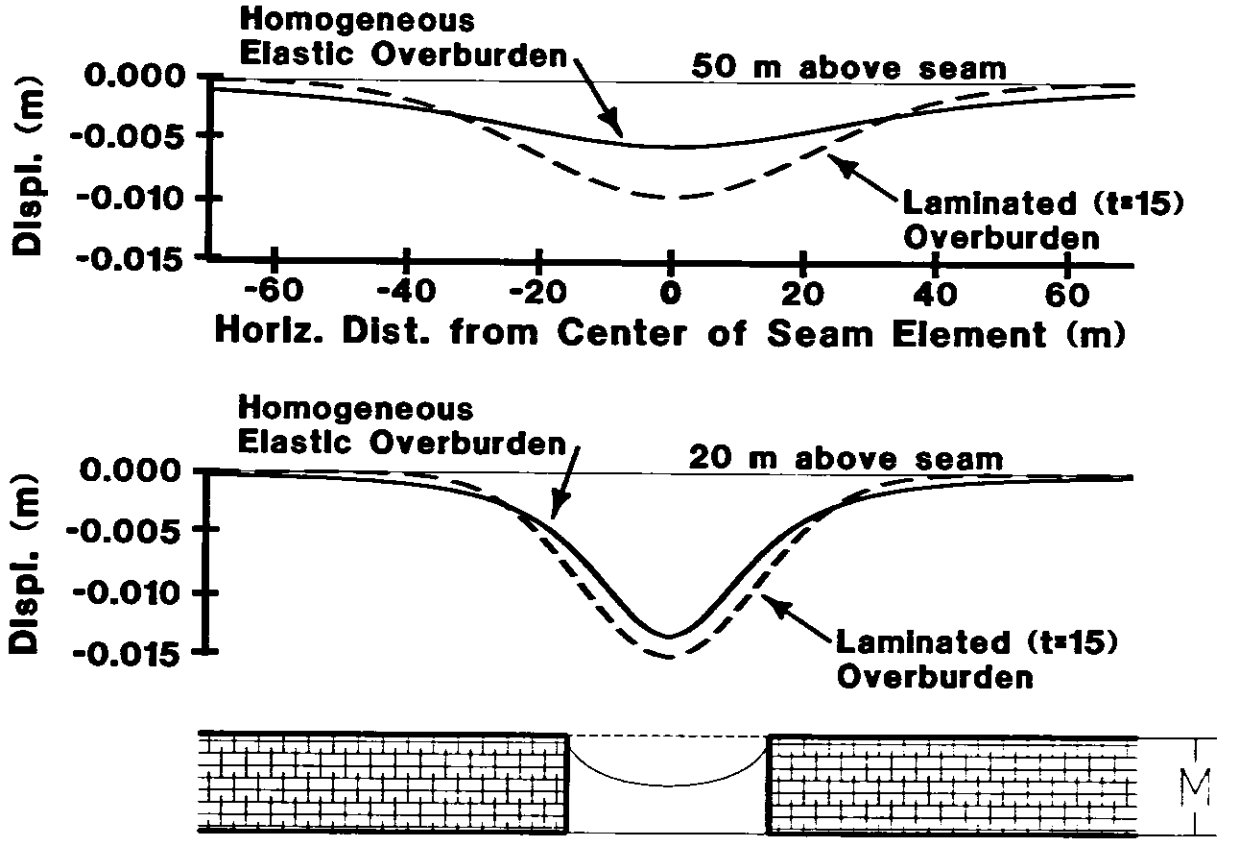

Figure 4.—Remote displacement due to a unit volume displacement.

curve. In earlier work where the laminated model was fit to several different individual sets of subsidence data [Yang 1992], a factor, ω:

$$\omega = \sqrt{\frac{H}{2\lambda}}, \qquad (18)$$

was found to be fairly constant at an average of 6.9. (Here, H is the overburden depth, and λ is defined in equation 5.) For the fitted subsidence curve from the laminated model in figure 6, the value of ω is 7.1, which agrees very well with this previous work.

For the subsidence curve from the homogeneous elastic overburden, the elastic modulus was lowered in an attempt to fit the empirical curve. However, long before the maximum surface subsidence from the model matched the maximum empirical surface subsidence, the convergence in the seam exceeded the seam thickness. The homogeneous elastic surface subsidence actually plotted in figure 6 was determined using an elastic modulus of 1 GPa (145,000 psi). From this curve, it is clear that the homogeneous isotropic surface subsidence is naturally much shallower and broader than the empirical data, and with only one effective variable parameter (E), the homogeneous isotropic model cannot be accurately fitted to the Northern Appalachian data. This result further confirms earlier indications that the homogeneous isotropic elastic overburden could not be made to fit subsidence data in the United Kingdom [Berry and Sales 1961; Salamon 1963].

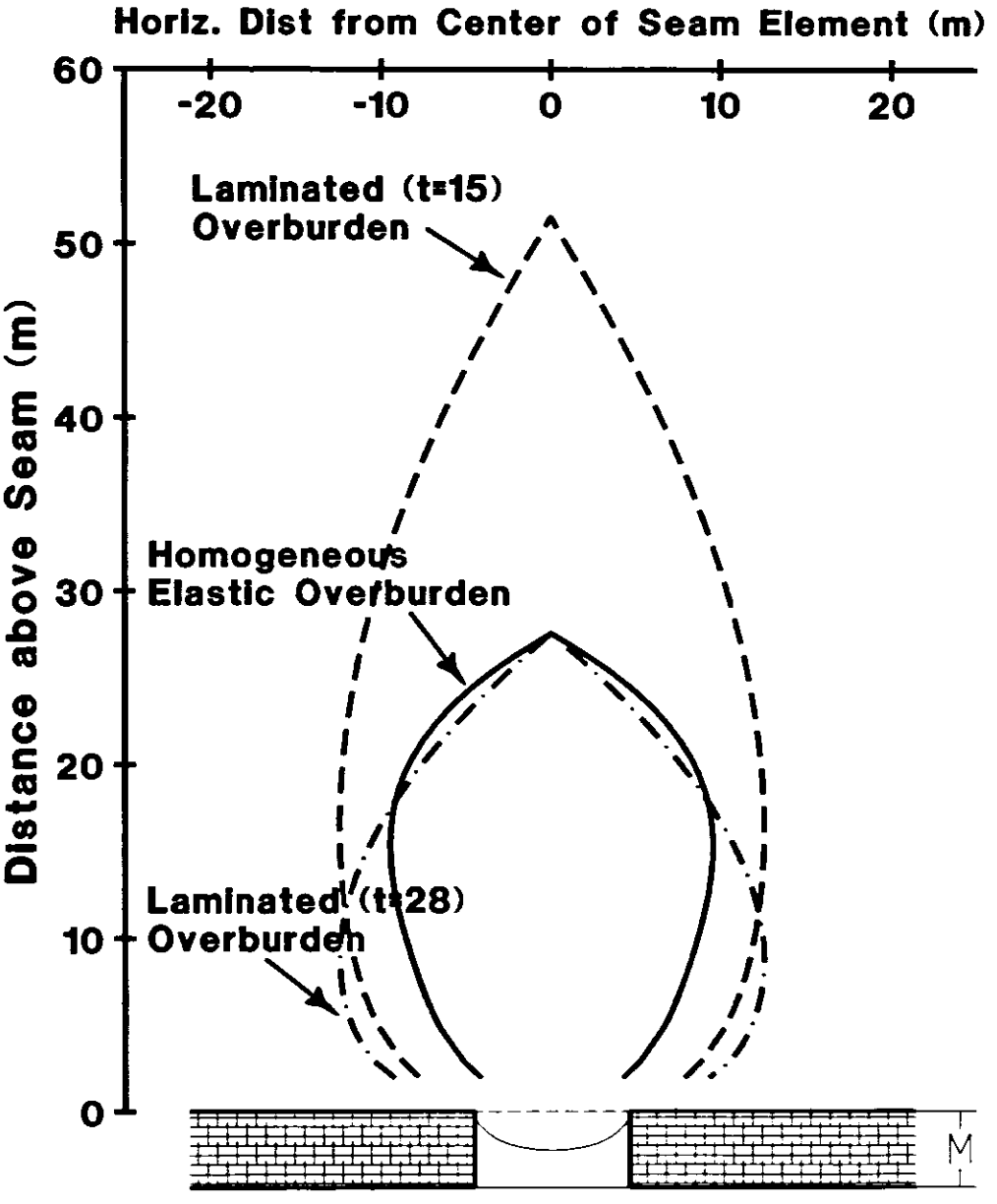

Figure 5.—1-cm (0.39-in) displacement contours associated with a unit volume displacement.

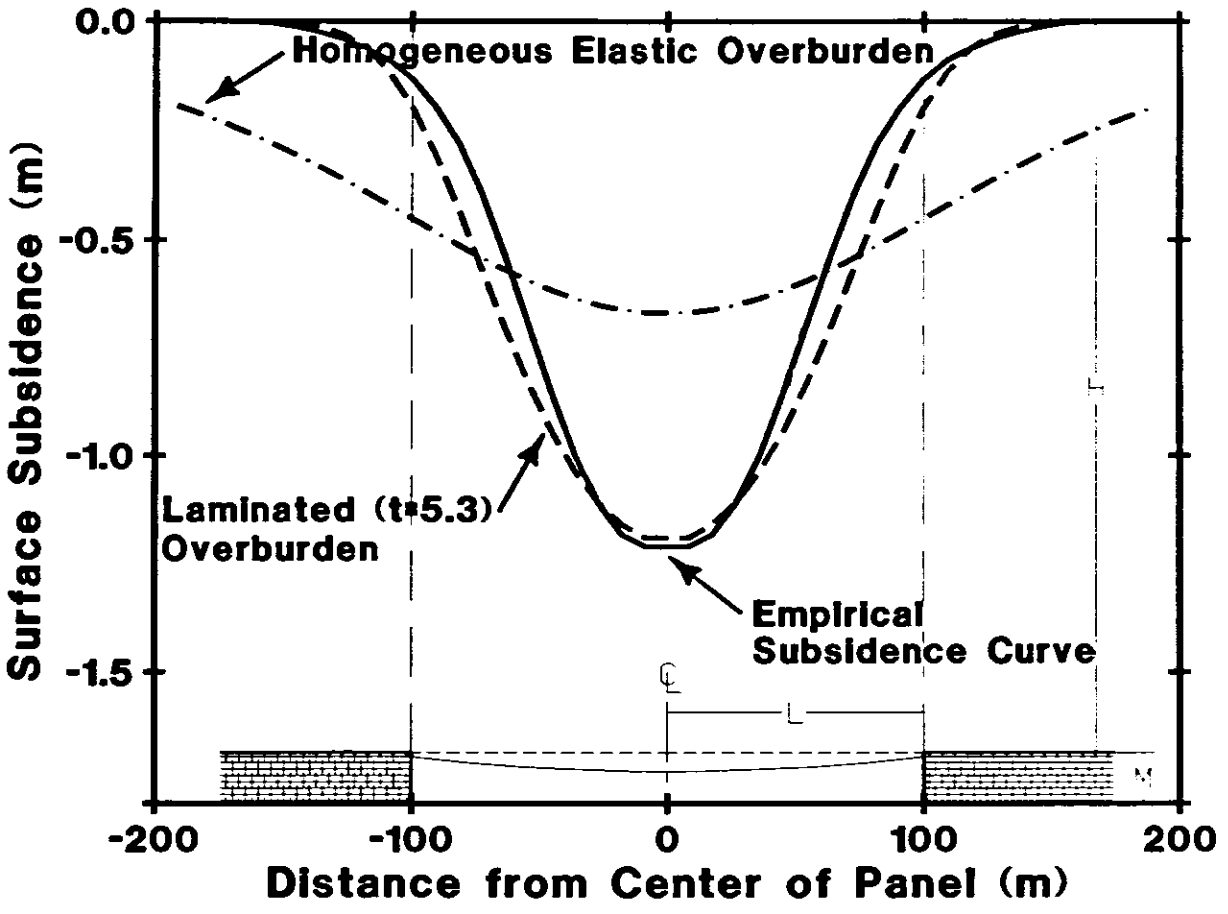

Figure 6.—Plot of the laminated and homogeneous isotropic subsidence fitted to the empirical curve.

THE LAMINATED MODEL PROGRAM, LAMODEL

IMPLEMENTATION FEATURES

The laminated overburden model, as presented in the previous sections of this paper, has been implemented into a modern boundary-element computer program called LAMODEL. This implementation has numerous practical features, including—

- Single- and multiple-seam simulations.
- Numerous individual excavation steps.
- Infinite media or surface effects for shallow seams.
- A constant overburden or a variable topography.
- Seam-level convergence and stress calculation, with each of the individual stress components (overburden, material, interseam, and surface) separately tabulated.
- User-defined laminae properties (elastic modulus, Poisson's ratio, and thickness).
- Up to 26 different in-seam materials can be specified from a selection of material models, which include elastic, elastic-plastic, strain-softening, bilinear strain-hardening, and exponential strain-hardening.
- User-defined convergence criteria.
- Grid sizes limited solely by the computation requirements (practical limit: 300 by 300).
- Either rigid or symmetric boundary conditions.
- Graphical pre- and postprocessors for simplified input entry and output analysis.

CASE STUDY

As part of the initial investigation and validation of this new implementation, the underground stresses, displacements, topographic stresses, and interseam interactions were modeled at a field site. This case study site is a multiple-seam situation

in eastern Kentucky. The geology in this area is fairly typical of the Southern Appalachian Coal Basin, with various sedimentary layers of sandstones, siltstones, shales, and numerous coal seams. The topography in the area is very rugged, with various steep ridges and valleys that have a topographic relief of over 600 m (2,000 ft). At the case study site, the overburden averages about 240 m (800 ft), but ranges from 90 m (300 ft) at the southeastern corner of the site to over 360 m (1,200 ft) at the northwestern corner (figure 7). (Because of the steep topography, it was critical to include the

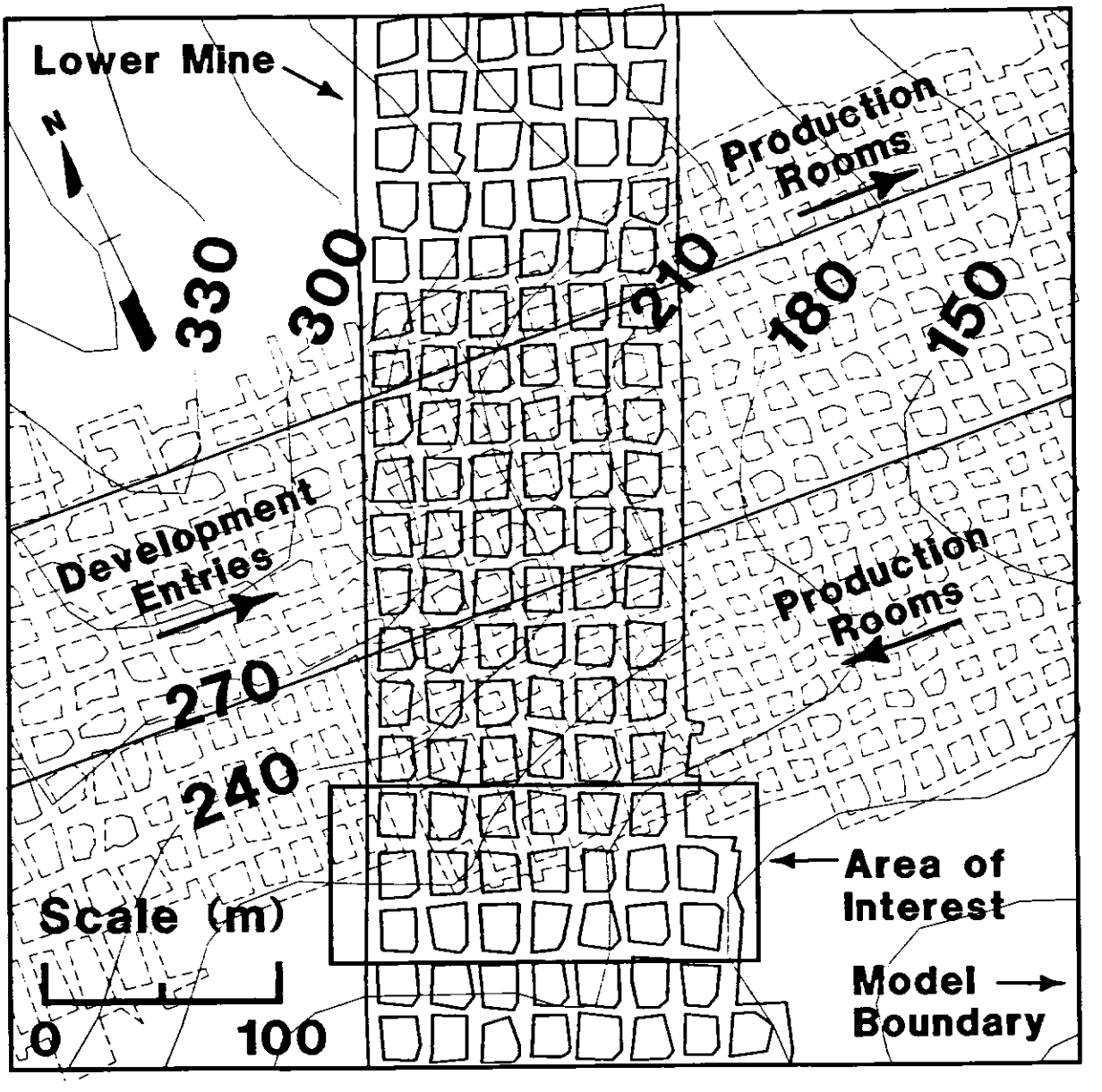

Figure 7.—Map of case study mines in eastern Kentucky.

topographic stress effects in the model to obtain accurate results.)

The overlying mine operates in the Upper Darby Seam, which typically averages about 2.0 m (6.5 ft) thick; however, in the model area, the extraction thickness had increased to over 2.7 m (9 ft). The lower mine operates in the Kellioka Seam, which averaged about 1.5 m (5.0 ft) thick in the study area. The interburden between the mines averages around 14 m (45 ft) and consists of interbedded sandstones and shales. The core logs nearest to the study site indicate about 3.5 to 5 m (12 to 15 ft) of thinly laminated shaley/carbonaceous sandstone (stack rock) directly over the Kellioka Seam. This is then overlain by 7.5 to 10.5 m (25 to 35 ft) of interbedded sandstones and shales, with shale primarily forming the floor of the Upper Darby Seam.

Both mines are room-and-pillar drift mines and utilize continuous miners for coal extraction. In some production sections, depending on local mining conditions, the mines remove the pillars on retreat for full extraction. In the study area, the lower mine had driven a seven-entry-wide set of main entries from north to south with pillars on 21- by 24-m (70- by 80-ft) centers and 6-m (20-ft) wide entries. Subsequently, the upper mine drove a seven-entry-wide set of panel development entries roughly perpendicular across the lower mains (figure 7). Relatively short (one- to two-crosscut) production rooms were driven to the north of the upper mine development entries during advance. At this point, no appreciable stress interaction was observed. Then, as the upper mine was pulling out of the section, long (seven- to eight-crosscut) production rooms with pillars on 18- by 18-m (60- by 60-ft), and smaller, centers were driven on the south side of the development entries (figure 7). At the extent of mining shown in figure 7, the upper mine began to experience major problems with pillar failure and floor heave and was forced to abandon the section.

Coincident with the failures in the upper mine, the lower mine experienced ground control problems in areas directly underlying the boundaries of the upper panel. These problems were primarily manifested as increased pillar spalling for approximately 30 m (100 ft) of entry and major roof cracking at overmined intersections. Both of these ground control problems were mitigated by supplemental bolting and cribbing.

The new laminated model, LAMODEL, was applied at this site to both quantify the magnitude of the stress interaction between the seams and to correlate the model results with in-mine ground control problems for subsequent predictions of mining conditions in future mine planning analysis. In the model, the seams were discretized with 3-m (10-ft) elements on 150-by-150 grids with the extent as shown in figure 7. Symmetrical seam boundary conditions were set, and no free-surface effects were included. The interburden was set at 14 m (45 ft), and the rock mass was simulated with a modulus of 20,700 MPa (3 million psi) and 15-m (50-ft) thick laminations. A strain-softening material was used for the in-seam coal, and the peak strength of the coal was varied until the pillars in the upper seam had just reached failure.

Additionally, because of the high topographic relief at the site, the topography was discretized with 15-m (50-ft) elements for an area extending 300 m (1,000 ft) beyond the limits of the displacement-discontinuity grids. The importance of including the topographic stress effects in the model is clearly evident in figure 8, which shows the topographic stress at the level of the upper mine. It is interesting to note in this figure the amount to which the topographic stress is "smoothed" with depth in comparison with the original topography shown in figure 7. Also, it should be observed in figure 8 that near the boundary of the upper mine (the area of interest) the topographic stress varies about 1.4 MPa (200 psi), or 30%, across the pillars in the lower mine.

The primary results of this multiple-seam modeling effort are shown in figure 9. Figure 9*C* shows the stress concentrations on the lower seam resulting from the pillar failure in the upper seam. In this image, stress concentrations up to 4.5 MPa (650 psi) and with functional widths of between 9 to 37 m (30 to 120 ft) can be seen. This model response correlates well with the underground observations. The calculated seam interaction stress results in increases of the average pillar stress in the lower mine up to 55% (figures 9*A* and 9*B*). By correlating this 55% increase in pillar stress with the observed ground control problems underground (figure 9), the magnitude of future ground control problems at this site can now be more accurately determined using LAMODEL.

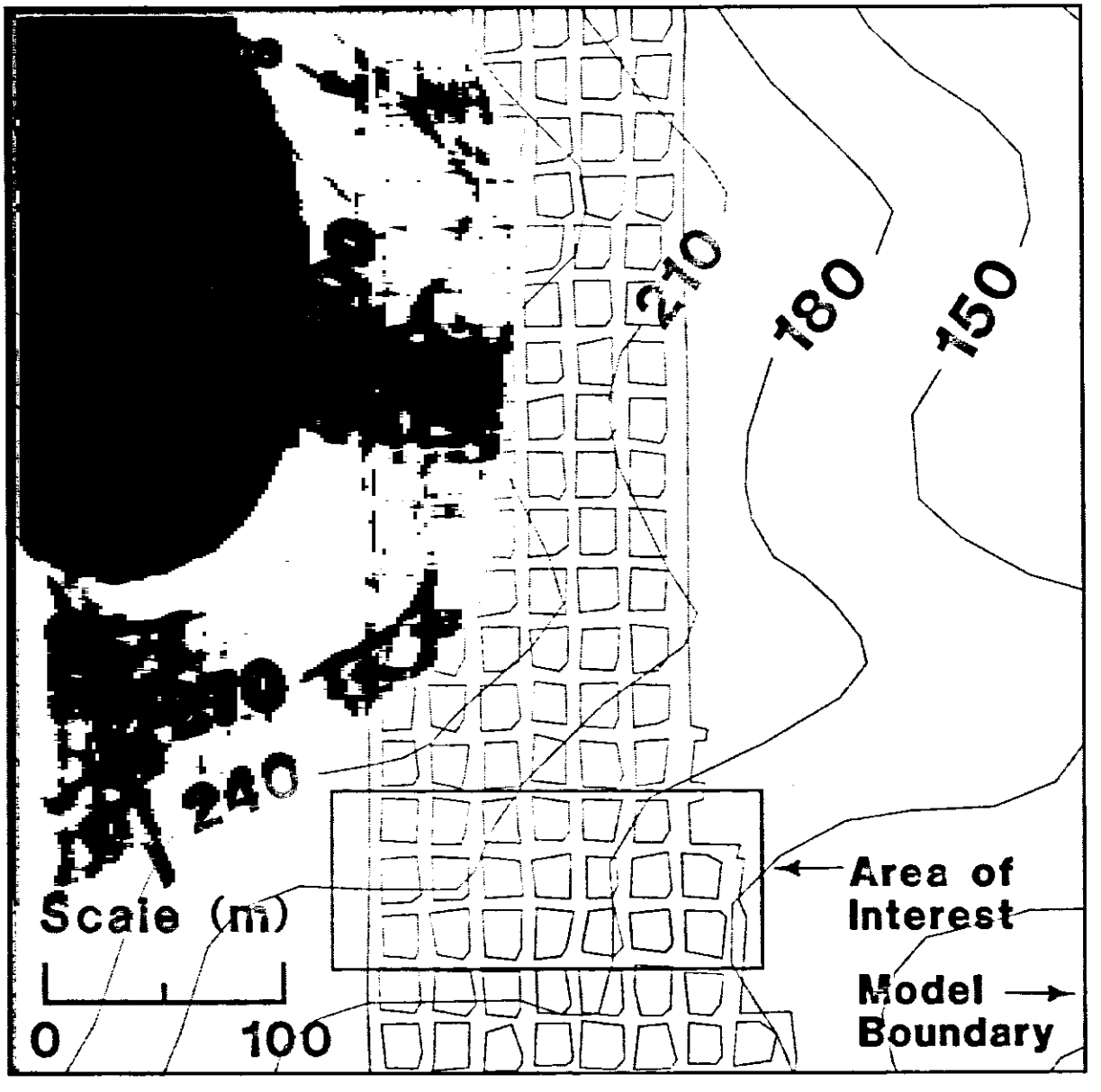

Figure 8.—Topographic stress on lower seam.

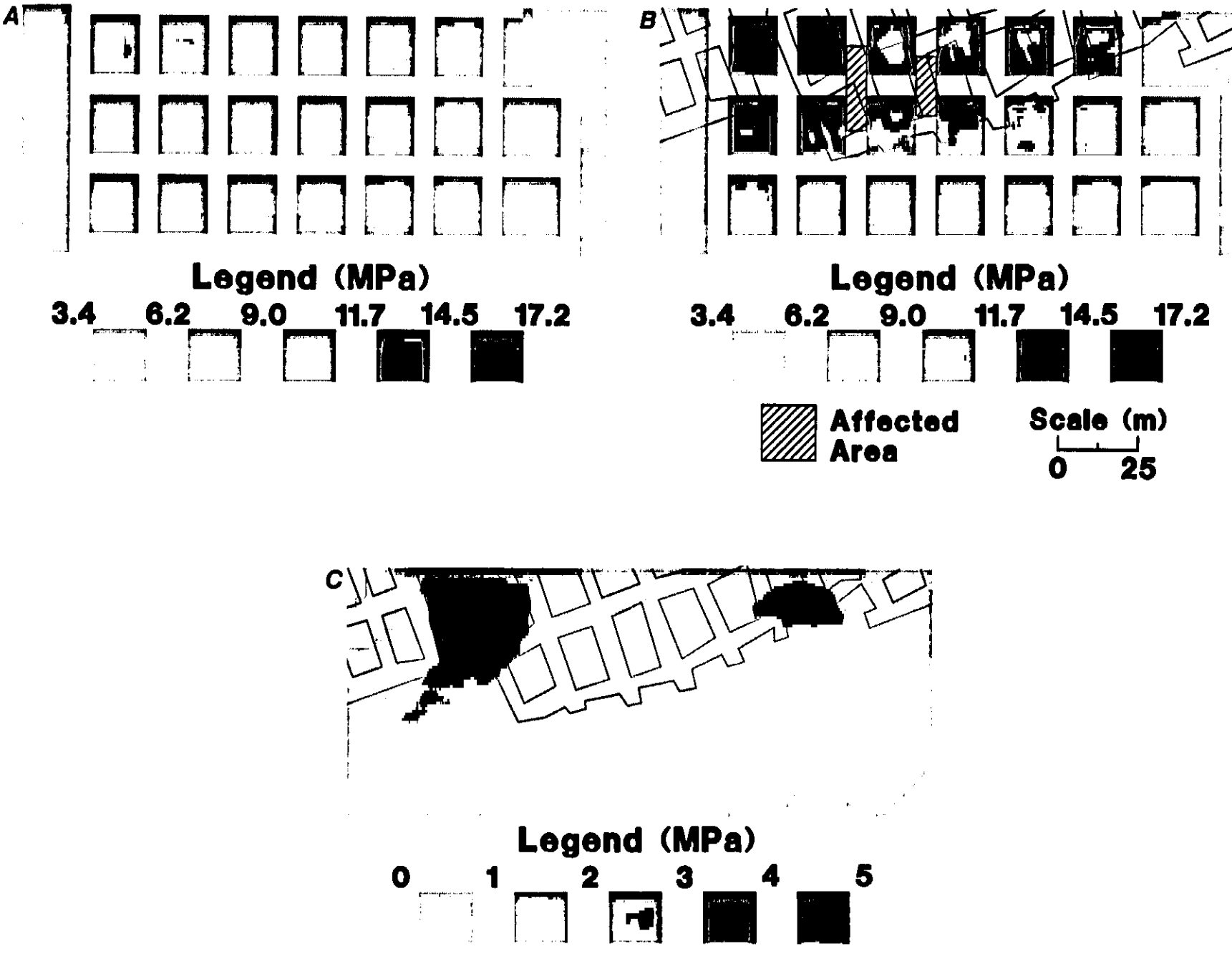

Figure 9.—Stress analysis on lower mine. *A*, single-seam stress; *B*, multiple-seam stress; *C*, additional stress from upper seam.

SUMMARY AND CONCLUSIONS

The investigation of the fundamental behavior of the laminated overburden presented in the first part of this paper has produced a number of significant results. First, it is clear that the laminated overburden (with a low lamination thickness) is more flexible or supple than the homogeneous isotropic overburden. This increased suppleness is evident in the greater convergence across a longwall panel, in the larger extent of the remote displacement contours, and in the nature of the surface subsidence. Second, due to the larger extent of the remote displacement contours, it is clear that a multiple-seam mine model using the laminated overburden will show increased interseam displacements and stresses compared with a homogeneous isotropic overburden. Third, because the overburden in the laminated model is effectively described with two parameters (as opposed to one parameter in the homogeneous isotropic model) and therefore provides two degrees of freedom for fitting observed data, the laminated model was capable of closely matching the observed abutment stresses and surface subsidence. In fact, the laminated model was easily fit to the observed surface subsidence, whereas the subsidence for the homogeneous isotropic overburden was fundamentally different from the observed subsidence.

In the second part of this paper, a new laminated displacement-discontinuity program, LAMODEL, was presented. This new program, in addition to the laminated overburden, also implements a number of innovative features, including topographic stress calculations, various in-seam material models, and variable boundary conditions at the seam level. In order to evaluate the accuracy and utility of the new model, it was used in a case study of a multiple-seam mining situation in steep topography. At this site, the ability of LAMODEL to include topographic stress effects, strain-softening coal, and symmetric boundary conditions greatly increased the realism and accuracy of the model. By correlating the LAMODEL results with the observed ground control problems, mine management will be better able to design and plan for future multiple-seam interactions. Because of the realistic flexibility of the laminated overburden model and the utility of the numerous practical features implemented in the new program, it appears that LAMODEL can provide realistic stress and displacement calculations for a wide range of mining situations.

REFERENCES

Berry DS [1960]. An elastic treatment of ground movement due to mining - part I. Isotropic ground. J Mech Physics of Solids *8*:280-292.

Berry DS, Sales TW [1961]. An elastic treatment of ground movement due to mining - part II. Transversely isotropic ground. J Mech Physics of Solids *9*:52-62.

Cook NGW, Hoek E, Pretorious JPG, Ortlepp WD, Salamon MDG [1966]. Rock mechanics applied to the study of rock bursts. J South Afr Inst Min Metall *66*:436-528.

Crouch SL [1976]. Analysis of stresses and displacements around underground excavations: an application of the displacement discontinuity method. Minneapolis, MN: University of Minnesota, Department of Civil Engineering, Geomechanics Report.

Crouch SL, Fairhurst C [1973]. The mechanics of coal mine bumps and the interaction between coal pillars, mine roof, and floor. U.S. Department of the Interior, Bureau of Mines, OFR 53-73.

Heasley KA, Zelanko JC [1992]. Pillar design in bump-prone ground using numerical models with energy calculations. In: Iannacchione AT, Mark C, Repsher RC, Tuchman RJ, Jones CC, comp. Proceedings of the Workshop on Coal Pillar Mechanics and Design. Pittsburgh, PA: U.S. Department of the Interior, Bureau of Mines, IC 9315, pp. 50-60.

Jaeger JC, Cook NGW [1979]. Fundamentals of rock mechanics. London: Chapman and Hall.

Jeran PW, Adamek V, Trevits MA [1986]. A subsidence prediction model for longwall mine design. In: Proceedings of the Longwall U.S.A. Conference. Pittsburgh, PA: pp. 101-112.

Kripakov NP, Beckett LA, Donato DA, Durr JS [1988]. Computer-assisted mine design procedures for longwall mining. Pittsburgh, PA: U.S. Department of the Interior, Bureau of Mines, RI 9172.

Mark C [1990]. Pillar design methods for longwall mining. Pittsburgh, PA: U.S. Department of the Interior, Bureau of Mines, IC 9247.

Plewman RP, Deist FH, Ortlepp WD [1969]. The development and application of a digital computer method for the solution of strata control problems. J South Afr Inst Min Metall *70*(9):33-44.

Salamon MDG [1961]. An introductory mathematical analysis of the movements and stresses induced by mining in stratified rocks. Durham, United Kingdom: King's College, University of Durham, Department of Mining, Research Report *9*:Bull 3.

Salamon MDG [1962]. The influence of strata movement and control on mining development and design [Thesis]. Durham, United Kingdom: University of Durham, Department of Mining.

Salamon MDG [1963]. Elastic analysis of displacements and stresses induced by the mining of seam or reef deposits, part I. J South Afr Inst Min Metall *63*(4):128-149.

Salamon MDG [1964]. Elastic analysis of displacements and stresses induced by the mining of seam or reef deposits, part II. J South Afr Inst Min Metall *64*(6):197-218.

Salamon MDG [1974]. Rock mechanics of underground excavations. In: Proceedings of the 3rd Congress, International Society for Rock Mechanics. Denver, CO: National Academy of Sciences, *1*(b)951-1099.

Salamon MDG [1989a]. Some applications of the frictionless laminated model. In: Proceedings of the 30th U.S. Symposium on Rock Mechanics. Morgantown, WV: West Virginia University, pp. 891-898.

Salamon MDG [1989b]. Subsidence prediction using a laminated linear model. In: Proceedings of the 30th U.S. Symposium on Rock Mechanics. Morgantown, WV: West Virginia University, pp. 503-510.

Salamon MDG [1991]. Deformation of stratified rock masses: a laminated model. J South Afr Inst Min Metall *91*(1):9-26.

Sinha KP [1979]. Displacement discontinuity technique for analyzing stresses and displacements due to mining in seam deposits [Thesis]. Minneapolis, MN: University of Minnesota.

Yang G [1992]. Numerical approach to the prediction of subsidence due to longwall coal mining using a laminated model [Thesis]. Golden, CO: Colorado School of Mines.

Zipf RK Jr., Heasley KA [1990]. Decreasing coal bump risk through optimal cut sequencing with a non-linear boundary element program. In: Hustrulid WA, Johnson GA, eds. Proceedings of the 31st U.S. Symposium on Rock Mechanics. Golden, CO: Colorado School of Mines, pp. 947-954.